



HAL
open science

A 2-D continuum model of a mixture of bone tissue and bio-resorbable material for simulating mass density redistribution under load slowly variable in time

Ugo Andreaus, Ivan Giorgio, Tomasz Lekszycki

► To cite this version:

Ugo Andreaus, Ivan Giorgio, Tomasz Lekszycki. A 2-D continuum model of a mixture of bone tissue and bio-resorbable material for simulating mass density redistribution under load slowly variable in time. *Journal of Applied Mathematics and Mechanics / Zeitschrift für Angewandte Mathematik und Mechanik*, 2014, 94 (12), pp.978-1000. 10.1002/zamm.201200182 . hal-00842604

HAL Id: hal-00842604

<https://hal.science/hal-00842604>

Submitted on 8 Jul 2013

HAL is a multi-disciplinary open access archive for the deposit and dissemination of scientific research documents, whether they are published or not. The documents may come from teaching and research institutions in France or abroad, or from public or private research centers.

L'archive ouverte pluridisciplinaire **HAL**, est destinée au dépôt et à la diffusion de documents scientifiques de niveau recherche, publiés ou non, émanant des établissements d'enseignement et de recherche français ou étrangers, des laboratoires publics ou privés.

A 2-D continuum model of a mixture of bone tissue and bio-resorbable material for simulating mass density redistribution under load slowly variable in time

Ugo Andreus¹, Ivan Giorgio^{2,4}, and Tomasz Lekszycki^{3,4}

¹ Dipartimento di Ingegneria Strutturale e Geotecnica, Facoltà di Ingegneria Civile e Industriale - Università di Roma La Sapienza, Via Eudossiana 18, 00184 - Roma, Italia

² Dipartimento di Ingegneria Meccanica e Aerospaziale, Facoltà di Ingegneria Civile e Industriale - Università di Roma La Sapienza, Via Eudossiana 18, 00184 - Roma, Italia

³ Warsaw University of Technology, Narbutta 85, 02-524 Warszawa, Poland

⁴ International Research Center "M&MoCS" Università degli studi dell'Aquila, Palazzo Caetani, 04012 - Cisterna di Latina, Italia

Key words Coupling between mechanics and biological stimuli, Artificial bio-resorbable material, Continuum mixture model, Load-induced replacement of artificial material with natural bone tissue, ODEs governing growth/resorption.

The bio-mechanical phenomena occurring in bones grafted with the inclusion of artificial materials demand the formulation of mathematical models which are refined enough to describe their not trivial behavior. A 3D theoretical model, previously developed and used in 1D space, is employed to investigate and explain possible effects resulting from 2D interactions, which may not be present in 1D case so more realistic situations are approached and discussed. The enhanced model was used to numerically analyze the physiological balance between the processes of bone apposition and resorption and material resorption in a bone sample under plain stress state. The specimen was constituted by a portion of bone living tissue and one of bio-resorbable material and was acted by an in-plane loading condition. The signal intensity between sensor cells and actor cells was assumed to decrease exponentially with their distance; the effects of adopting two different laws, namely an absolute and a quadratic functions, were compared. Ranges of load magnitudes were identified within which physiological states are established. A parametric analysis was carried out to evaluate the sensitivity of the model to changes of some critical quantities within physiological ranges, namely resorption rate of bio-material, load level and homeostatic strain. In particular the spatial distribution of mass densities of bone tissue and of resorbable bio-material and their time evolution were considered in order to analyze the biological effects due to the parameter's changes. Synthetically, these biological effects can be associated to different ratios between bone and bio-material densities at the end of the process and to different delays in the bone growth and material resorption. These numerical analyses allowed for finding the most desirable situations in which a gradual resorption of the artificial graft occurs together with the simultaneous formation of new bone, finally leading to an almost complete substitution of the bio-resorbable material with living tissue.

1 Introduction

It has been known for a very long time that bone tissue adapts to functional stress by changes in structure and mass. Nulend et al. studied the response of isolated chicken osteocytes to intermittent hydrostatic compression as well as pulsating fluid flow, and the results supported the hypothesis that stress on bone causes fluid flow in the lacunar-canalicular system, which stimulates the osteocytes to produce factors that regulate bone metabolism [29]. Strain-derived flow of interstitial fluid through this porosity seems to mechanically activate the osteocytes, as well as ensure transport of cell signaling molecules, nutrients, and waste products [28]. Although tissue strain and fluid shear stress both cause cell deformation, these stimuli could excite different signaling pathways. This is confirmed by the experimental findings of Mullender et al., in human bone cells, that strain applied through the substrate and fluid flow stimulate the release of signaling molecules to varying extents [42]. A topical and intriguing problem concerns the study referring to a bio-resorbable material that upon placement within the human body starts to dissolve (resorbed) and is slowly replaced by advancing bone tissue [9]. Common examples of bio-resorbable materials are tricalcium phosphate [$Ca_3(PO_4)_2$] and polylactic-polyglycolic acid copolymers. Calcium oxide, calcium carbonate and gypsum are other common materials that have been utilised during the last three decades [19, 25, 30, 43]. While replacements made of titanium merely plug holes, a new kind of degradable implant stimulates the body to regenerate itself: it is custom-fit and disappears to the same extent that the bone regrows. As for rate of degradation, implant should degrade at the rate the tissue heals [7]. In contrast to long-term solutions based

on titanium, degradable implants are intended to replace the missing pieces of bone only until the fissure closes itself up. That may last months or even years, depending on the size of the defect, the age and health status of the patient. Implant of new generation improve the conditions for the healing process. Unlike the conventional bony substitutes to date, they are not made up as a solid mass, but are porous instead. Precise little channels permeate the implant at intervals of just a few hundred micrometers. The porous canals create a lattice structure which the adjacent bones can grow into [33]. But the material can only be applied in places where it will not be subject to severe stress [17, 19, 30]: thus, these kind of implants will primarily replace missing facial, maxillary and cranial bones [23, 26, 44]. Currently, they are able to close fissures of up to 25 square centimeters in size. Bioresorbable materials are extensively used for a wide range of biomedical applications from drug delivery to fracture fixation [9, 55, 56], and may remain in the body for weeks, months or even years. Perhaps the best-known use for bio-resorbables is in sutures, but they are also used in a wide range of other medical implants where temporary fixation of tissue is required, suture anchors, meniscal tacks and interference screws made from bioresorbable polymers and bioresorbable bone graft substitute materials [7, 54], the local treatment of osteoporosis (osteoplasty) [58], temporary scaffolds which provide support until the tissue heals and which actively enhance the speed and/or quality of tissue repair [33]. In the recent past various models and methods have been developed and published to numerically simulate the phenomenon of bone formation compared with resorption of the biomaterial. Wang et al. presented a phenomenological diffusion-reaction model for the biodegradation of biodegradable polymers. The biodegradation process is modelled using a set of simplified reaction-diffusion equations. The equations are firstly solved for simple cases of plates and pins. The diffusion-reaction equations are solved using the finite element method for strip and square meshes, showing how the model can be used to assist the design of sophisticated fixation devices [60]. Han et al. completed the model of biodegradation for biodegradable polymers that was previously developed by [60], considering crystallization during biodegradation that was not considered in the previous work [20]. Wang et al. presented a model for the change in Young's modulus of biodegradable polymers due to hydrolysis cleavage of the polymer chains [59]. The model is based on the entropy spring theory for amorphous polymers. The experimental data obtained by [57] for poly(L-lactic acid) and poly(D-lactic acid) are examined using the model. The governing equations for biodegradation and the relation between Young's modulus and average molecular weight can be combined to calculate the load transfer from a degrading device to a healing bone. Pan et al. presented an understanding of the saturation behaviour observed when incorporating tricalcium phosphate in various polyesters to control the degradation rate using a mathematical model [45]. Carbonate Apatite (CA) ceramics have the potential to be used for bone tissue regeneration. Of special significance is the ability of CA ceramics to support the growth and differentiation of osteoclasts and osteoblasts. The fact that calcium carbonates, such as calcite and aragonite are resorbed by osteoclasts [24] suggests that the presence of carbonate in the substrates plays an important role in osteoclastic resorption [27]. Madeo et al. in [36] introduced a two-constituent porous continuum as a model describing the long-term growth/resorption phenomena in bone tissues grafted with bio-resorbable materials as driven by mechanical loads, under the assumption of first-order deformation theory. Madeo et al. in [35] presented an improvement of the previous model [36] under the assumption of second-gradient deformation theory. Some numerical simulations for rod-bones subjected to axial external load are presented in [35, 36]. Lekszycki et al. in [32] presented a continuum poro-elastic mixture model in which two apparent mass densities are introduced to describe, at a macroscopic length scale, situations in which bone tissues and artificial materials coexist and interact. To account for resorption and synthesis phenomena in one dimensional cases, suitable evolution equations are introduced for Lagrangian apparent mass densities of the mixture constituents in which an integrodifferential operator defined on deformation fields appears. Moreover, understanding and predicting the adaptation properties of living bone are particularly important for proper design of prosthetic devices in contact with bone *e.g.* fracture fixation plates, surgical screws, and artificial joints [1, 5, 22]. If orthopaedic implants place a different stress from the one that the bone tissue is accustomed to, the functional adaptation is activated. The remodelled bone tissue could be weaker and lead to failure of the surgical procedure. Some authors assumed that bone remodelling rule was represented by the classical proportional-integral-derivative (PID) control, applied to the error signal between the strain energy density and a target to be optimized; the underlying premise was that the mass should be distributed in an efficient way, therefore using a minimum amount of material to accomplish the mechanical function, in which stiffness and mass are conflicting objectives [2–4]. In this paper is assumed that a simple network of sensors measures the mechanical stimulus and “directs” the actions of active cells. The artificial material we assume to use is absolutely not active in both sensing and actuating process. However one could conceive an “intelligent” bioresorbable material having much more effective performances by using the concept developed in [6, 14, 15, 18, 38, 40, 49, 50]. In this paper reference is made to earlier works by [36] and [32], where a model which applies to 3D case was proposed and numerical examples were performed in 1D space to investigate and explain some fundamental mechanisms possible during remodeling process. Herein possible effects resulting from 2D interactions are being discovered and examined which may not be present in 1D case so more realistic situations are approached and discussed. The aim was to describe some of the complex bio-mechanical phenomena which occur in bones tissues when they are reconstructed or reinforced by the addition of an artificial resorbable material. In fact, in bones grafted with bone-substitute bio-resorbable artificial materials the living bone tissue is synthesized or resorbed and

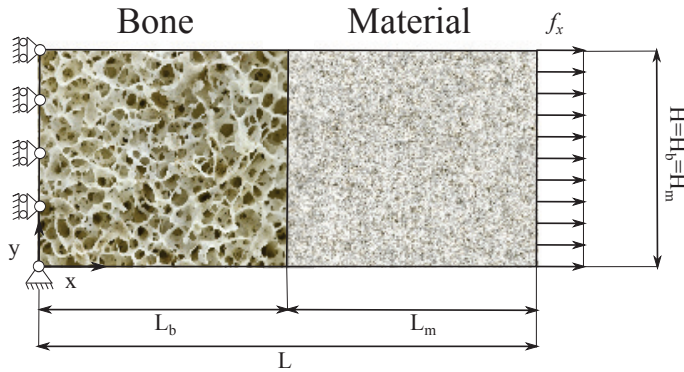


Fig. 1 Schematic presentation of 2D model considered in numerical examinations. Interface and its close environment of connected two different materials namely, bone tissue (left) and bone-substitute (right) is presented. The lengths $L_b = L_m$ are of the magnitudes comparable to $5D$ where D denotes a characteristic distance of osteocyte influence.

the artificial material is resorbed and possibly replaced by a living tissue. The density of deformation energy is assumed as a driving signal for remodeling. The aim of this paper is to determine under which conditions the mechanisms driving the natural functional adaptation process still are able to produce their beneficial effects also in presence of grafted materials in reconstructed bones. As it is clinically observed that sometimes grafted materials may be too quickly completely resorbed thus leaving voids in reconstructed bones, we want to determine in which conditions and to what extent the action of functional adaptation will lead to a replacement of bio-resorbable material with bone tissue or at least to the final constitution of a stable composite.

2 Model and Materials

2.1 Solid mixture of bone tissue and bio-resorbable material

The considered solid material is constituted by a mixture of bio-resorbable material (of the type used in bone reconstructive surgery) and living bone-tissue. In the remainder of the text it is agreed that the mass density of the bone tissue, of the bio-material and of the mixture must be understood as apparent mass density. Indeed, it is well-known that at least the deformation in bone-tissue is a physical quantity of relevance in the resorption/synthesis phenomena arising in it. Similarly, it will be of relevance in the considered mixture composed by bio-material and living bone-tissue, this last being the only which is carrying the sensor cells. These last, after having measured the strain energy, will convey a suitable stimulus to the actor cells which are assumed able to be activated whenever in the whole bone tissue/bio-material mixture the values of “effective” porosity allow the deposition of precursor cells. Thus, a reference configuration Ω needs to be introduced to describe deformation occurring in considered solid mixture, together with the following referential fields, evaluated at the position \mathbf{X} (of the two-dimensional euclidean space) and at the time instant t :

- mass density of bone tissue, ρ_b ;
- mass density of bio-resorbable material, ρ_m ;
- mass density of the mixture, $\rho = \rho_b + \rho_m$;
- porosity of the bone tissue/bio-material mixture, *i.e.* the volume fraction which is not occupied by bone tissue or bio-material, ϕ ;
- Young’s modulus of bone tissue, Y_b ;
- Young’s modulus of bio-resorbable material, Y_m ;
- components of the displacement vector, u, v ;

- 2-D components of the small strain tensor,

$$\begin{aligned}\varepsilon_{xx} &= u_{,x} \\ \varepsilon_{yy} &= v_{,y} \\ 2\varepsilon_{xy} &= u_{,y} + v_{,x}\end{aligned}$$

- strain energy density (per unit area), U ;
- apposition-resorption stimulus, S , *i.e.* a scalar quantity which measures the activation signal collected at (\mathbf{X}, t) by the actor cells, that is osteoblasts (responsible for synthesis of bone tissue) and osteoclasts (responsible for resorption of bone tissue or bio-material);
- fraction of the active sensor cells, d , *i.e.* the number of active osteocytes over the number of potentially available osteocytes in the reference element of unitary volume centered at (\mathbf{X}, t) .

The above fields are limited by the upper bounds coinciding with the maximum values of the:

- mass density of bone tissue, $\rho_{b\text{Max}}$,
- mass density of bio-resorbable material, $\rho_{m\text{Max}}$,
- mass density of the mixture, $\rho_{\text{Max}} = \max\{\rho_{b\text{Max}}, \rho_{m\text{Max}}\}$, *i.e.* mixture density corresponding to vanishing porosity,
- Young's modulus of bone tissue, $Y_{b\text{Max}}$,
- Young's modulus of bio-resorbable material, $Y_{m\text{Max}}$,
- Young's modulus of the mixture, $Y_{\text{Max}} = \max\{Y_{b\text{Max}}, Y_{m\text{Max}}\}$, *i.e.* mixture Young's modulus corresponding to vanishing porosity.

Time variations of loads and of elastic moduli (which are determined by the corresponding variations of mass densities (see Eqs. (3) and (4)), *i.e.* by synthesis and resorption phenomena) occur in a time scale which is much larger than the transient characteristic time leading to macroscopic mechanical equilibrium. Therefore inertia effects can be neglected in the mechanical equilibrium and in the evolutionary problems considered here. Therefore the evolutionary equations for mass densities will be simply first order ordinary differential equations with respect to time.

2.2 Mechanical governing equations in weak form

Since the considered problem is time-dependent but the evolution in time is very slow the quasi-static formulation is assumed and the time is treated as a simple parameter. The solution is divided into two problems, classical formulation of static elastic problem and parametric evolution of material in time which provides supplementary formulas to the standard constitutive relations. The equations governing the mechanical problem can be expressed in weak form. The test functions are defined by the 2-D components δu , δv . The Theorem of Virtual Work is enforced on the whole domain:

$$\int_{\Omega} [\sigma_{xx}\delta u_x + \sigma_{yy}\delta v_y + \sigma_{xy}(\delta u_y + \delta v_x)] d\Omega - \int_{\Omega} [b_x\delta u + b_y\delta v] d\Omega - \int_{\partial\Omega_f} [f_x\delta u + f_y\delta v] d\partial\Omega = 0 \quad (1)$$

where Ω is the 2-D domain, $\partial\Omega_f$ is the boundary where the external force components are applied (right side in Fig. 1), b_x, b_y are the components of the volume force density, f_x, f_y are the components of the surface force density. On the constrained side (left side in Fig. 1), the boundary conditions are prescribed as $u = 0$ everywhere, $v = 0$ just in the lower left corner (see Fig. 1). Hence, the first term at the right hand side of Eq. (1) accounts for the balance of forces in the bulk. As for the boundary conditions, traction type conditions are assumed on the external boundary $\partial\Omega_f$ and continuity of forces (which also implies continuity of displacement) at any internal discontinuity surface inside Ω . It is worth to recall here that in the present treatment only mechanical boundary conditions are needed; therefore the bulk forces are assumed to be zero $b_x = 0, b_y = 0$.

2.3 Preliminary definitions

In this section the interaction between sensor cells and actor cells are specified (see [52]) as mediated by stimulus intensity. It is well-established (see e.g [11] and [52]) that sensor cells produce a signal which is sent to actor cells surrounding them. The overall signal collected by any actor cell is the stimulus it perceives. The signal depends on the deformation energy which is “*measured*” by sensor cells in the portion of tissue where they are placed. This signal reaches actor cells and drives their behavior and its intensity depends on the distance between sensor cells and actor cells. All these cause/effect relationships are modeled by means of suitable constitutive equations below. Another phenomenon to be accounted for by the proposed model concerns the effect of biological actions on mechanical behavior of the mixture of bone tissue and bio-material: these actions affect the mass densities of both materials, the mixture porosity and its elastic moduli. The listed cause/effect relationships are modeled by means of simple evolution equations, similar to those derived in [31] but extended to take into account i) the effects of “*effective*” porosity on cell activities, together with ii) the presence of artificial material in which the sensor cells are not present. The postulated equations allow us to simultaneously deal with resorption of both bio-material and bone tissue or with synthesis of bone tissue. On the other hand, suitable constitutive equations are introduced to model the relationships among biological and mechanical states, signal and stimulus, or stimulus and remodelling. In the following considerations we use apparent mass density for material characterization, according to the standard definition:

$$\rho = \gamma \varsigma \quad (2)$$

where γ is the mass density of the mineral matrix, and ς is the ratio of the volume occupied by the material matrix to the bulk volume. Since the mass density of considered composite cannot exceed the maximal density of a compact bone it is convenient to introduce the normalized mass densities representing contributions of components in the total mass of considered composite. Normalizing the mass densities of bone and material with respect to ρ_{Max} yields non-dimensional:

- mass density of bone, $\tilde{\rho}_b = \rho_b / \rho_{\text{Max}}$,
- mass density of material, $\tilde{\rho}_m = \rho_m / \rho_{\text{Max}}$,
- total mass density, $\tilde{\rho} = \tilde{\rho}_b + \tilde{\rho}_m$;

and normalizing the Young’s moduli of bone and material with respect to Y_{Max} gives non-dimensional Young’s modulus of bone tissue,

$$\tilde{Y}_b = Y_b / Y_{\text{Max}} = (\tilde{\rho}_b)^{\beta_b} \quad (3)$$

Young’s modulus of material,

$$\tilde{Y}_m = Y_m / Y_{\text{Max}} = (\tilde{\rho}_m)^{\beta_m} \quad (4)$$

where β_b and β_m are constants (see [11]). Young’s modulus of the mixture varies with mass density according to the following relation [11]:

$$Y = Y_{b\text{Max}} (\tilde{\rho}_b)^{\beta_b} + Y_{m\text{Max}} (\tilde{\rho}_m)^{\beta_m} \quad (5)$$

Thus, the corresponding dimensionless Young’s modulus takes the form:

$$\tilde{Y} = \tilde{Y}_{b\text{Max}} (\tilde{\rho}_b)^{\beta_b} + \tilde{Y}_{m\text{Max}} (\tilde{\rho}_m)^{\beta_m} \quad (6)$$

where $\tilde{Y}_{b\text{Max}} = Y_{b\text{Max}} / Y_{\text{Max}}$, $\tilde{Y}_{m\text{Max}} = Y_{m\text{Max}} / Y_{\text{Max}}$ and $\tilde{Y} = Y / Y_{\text{Max}}$.

Plane stress is defined according to the well-known following relations:

$$\sigma_{xx} = \frac{Y}{(1 - \nu^2)} (u_{,x} + \nu v_{,y}) \quad (7)$$

$$\sigma_{yy} = \frac{Y}{(1 - \nu^2)} (\nu u_{,x} + v_{,y}) \quad (8)$$

$$\sigma_{xy} = \frac{Y}{2(1 + \nu)} (u_{,y} + v_{,x}) \quad (9)$$

and the strain energy density is defined as:

$$U = \frac{1}{2} [\sigma_{xx}u_{,x} + \sigma_{yy}v_{,y} + \sigma_{xy}(u_{,y} + v_{,x})] \quad (10)$$

As for the fraction of sensor cells, the biological activity of a material particle of the bone/bio-material solid mixture is assumed to depend on its content of osteocytes. A material particle of the bone/bio-material solid mixture is assumed to be biologically active. Indeed in living bone tissue osteocytes are present. These are mechanosensation cells: they detect the deformation state in their neighbourhood. Osteocytes are cells which result from a biological transformation occurring in completely formed bone tissue: this tissue is built by osteoblasts, when a biological signal tells them that it is necessary to synthesize bone tissue. As soon as it is necessary to continue to build bone tissue, osteoblasts remain localized where they were deposited and go on synthesizing bone tissue. At a given moment an osteoblast is completely surrounded by bone tissue and it cannot synthesize any more. Then it becomes an osteocyte: its work will be to measure the strain-deformation energy in its neighbourhood and “to warn” all surrounding actor cells about the mechanical state of the part of bone tissue it is controlling. Therefore to describe some of the biological mechanisms occurring in bone/bio-resorbable material solid mixture we introduce a relation between the bone-tissue and bio-resorbable material mass densities and the density of active sensor cells, $d(\rho_b)$, *i.e.* the number of osteocytes per unit volume which are able to measure the mechanical state and send the signal which will act as stimulus for the actor cells (such sensor cells are present only in living bone-tissue) [32,36]:

$$d(\rho_b) = \eta \frac{\rho_b}{\rho_{Max}} = \eta \tilde{\rho}_b \quad (11)$$

with the parameter η ranging between 0 and 1 ($0 < \eta \leq 1$). Growth and remodelling of bone tissue are made possible by the action of osteoclasts and osteoblasts. These cells are formed, by means of some complex mechanisms, when and where synthesis or resorption of bone tissue are needed. The biological process leading to the activation of osteoclasts and osteoblasts involves the diffusion of their precursor cells through the bone-tissue. Physiologically bone-tissue is porous, and a fluid is filling its pores. This fluid transports the precursor cells. In order to be assured that the activation process leading to the formation and action of osteoclasts and osteoblasts is possible (*i.e.* in order to be sure that the bone/bio-material solid mixture is biologically active) one needs to be sure that such a mixture is porous, and its porosity allows for both i) the needed cell diffusion phenomena and ii) the nutrition supply associated with the development of a suitable vascular network. Moreover, the actor cells need to have pore surface where to sit in order to start their action. Since porosity is considered here as a correct measure of the available pore surface where actor cells may deposit, then it is a kinematical parameter which needs to be introduced if one wants to describe remodelling phenomena in living bone-tissues and also in bone/bio-material solid mixture. In this mixture if porosity is too low then living cells will not be able to efficiently resorb the resorbable material neither to form new bone tissue, as the available space will not allow for the action of a suitably large number of actor cells. If porosity, on the other hand, is too large then we do not have enough matter (*i.e.* bone tissue or bio-material) on which actor cells may deposit. Also in this circumstance remodelling will not occur quickly enough or will not occur at all. To describe the mechanical phenomena which influence the porosity variation in considered solid mixture a relation is introduced:

$$\phi(\rho_b, \rho_m) = 1 - \theta \frac{\rho_b + \rho_m}{\rho_{Max}} = 1 - \theta \tilde{\rho} \quad (12)$$

which links the “*effective porosity*” (effective for the deposit of actor cells) to mass densities; the parameter θ takes a value between 0 and 1, *i.e.* $0 < \theta \leq 1$.

2.4 Mechanical stimulus

The action of osteoclasts and osteoblasts is tuned by a biological stimulus. Similarly to what occurs in physiological bone-tissue, such a stimulus is assumed to be conveyed in every material particle of the bone/bio-material solid mixture by the surrounding osteocytes. The signal stemming from a sensor cell in a given material particle of the bone/bio-material mixture is assumed to be instantaneously transmitted (*i.e.* the transmission time scale is negligible when compared with the characteristic time of the remodeling phenomena) and its intensity is assumed to decay exponentially with the distance from it. Moreover, the signal sent by all sensor cells located in a given material particle is assumed to be of the same intensity, so that the total intensity of the signal sent by considered material particle is proportional to d ; it is obviously agreed that the parameter d is non-zero only where living bone tissue is present. Finally, all sensor cells are assumed to elaborate a signal which is proportional to the deformation energy density in the neighborhood of the position where they are located. In conclusion the following assumption does hold for the mechanical stimulus S :

$$S(\mathbf{X}, t) = \int_{\Omega} U(\mathbf{X}_0, t) d[\rho(\mathbf{X}_0, t)] e^{-f_i(\mathbf{X}-\mathbf{X}_0)} d\mathbf{X}_0 - P_{ref} = P(\mathbf{X}, t) - P_{ref}, \quad i = 1, 2 \quad (13)$$

In particular, two different attenuation laws of the signal were considered, namely the absolute exponential function of Eq. (14) and the quadratic exponential function of Eq. (15)

$$f_1(\mathbf{X} - \mathbf{X}_0) = \frac{\|\mathbf{X} - \mathbf{X}_0\|}{D} \quad (14)$$

$$f_2(\mathbf{X} - \mathbf{X}_0) = \frac{\|\mathbf{X} - \mathbf{X}_0\|^2}{2D^2} \quad (15)$$

where the length D represents the range of action of sensor cells; the attenuation laws will be improved in future by better elaboration of real mechanisms responsible for cells signaling. The value P_{ref}

$$P_{\text{ref}} = \int_{\Omega} U_{\text{ref}} d(\rho_{\text{b ref}}) e^{-f_i(\mathbf{X} - \mathbf{X}_{\text{ref}})} d\mathbf{X} \quad (16)$$

is the reference value of stimulus, associated with a biological equilibrium state for which the effect of resorption and synthesis are balanced; referring to Fig. 2, the coordinates of point \mathbf{X}_{ref} are chosen as $\{L/2, H/2\}$. The meaning of this reference value will become clear later, when a resorption-synthesis law will be formulated. For detailed discussion of the biological evidence which is the basis of the just formulated constitutive equation we refer to [11,52]. The non-dimensional stimulus can be defined as:

$$\tilde{S} = \frac{P - P_{\text{ref}}}{P_{\text{ref}}}$$

where P_{ref} corresponds to the homeostatic deformation ε_{ref} , *i.e.* the strain state where the osteoregulatory balance of the bone is maintained [51]. The osteocytes are hypothesized to act as sensors of a mechanical signal and regulators of bone mass by mediating the actor cells – the osteoblasts and osteoclasts. The mathematical model used to simulate this control process uses the strain energy density as the mechanical signal that the osteocytes appraise. The osteocytes, distributed through the bone in a particular pattern, emit a stimulus in their environments equivalent to the difference between the local strain energy density and a constant reference value. The actor cells regulate bone density in their area between zero and maximal density, dependent on the total stimulus they receive from the osteocytes, whereby the influence of an individual osteocyte stimulus diminishes exponentially according to its distance from the actor cell concerned. The definition of P_{ref} is an important criterion since regenerating aspects depend on it. For this reason, Sections 3.2 and 3.6.3 later on are devoted to analyze its influence on the results. In particular, in Sect. 3.2 a load level was assumed which causes an initial homeostatic deformation state, and hence an initial energy density approximately equal to the reference energy density. In Sect. 3.6.3 a sensitivity analysis to variation of the homeostatic strain and hence of the associated P_{ref} was performed, all other parameters being equal. The range between normal daily activity and less vigorous activity was investigated. The length L of the specimen was chosen as characteristic length scale, while the parameter D was assumed equal to $L/10$ in the performed numerical simulations.

2.5 Evolution rules

The mass density rates of bone tissue and bio-resorbable material are assumed to depend on the local value of the stimulus derived from the signals received from surrounding sensor cells, that is osteocytes. Since the bone remodeling is driven by mechanical loading exciting activities of cells synthesizing or removing intercellular matrix, it is assumed that the necessary supply or removal of associated molecules is possible that is the considered system has an ‘‘Open System’’ nature. Thus, the evolution equations for the mass densities can be written as:

$$\dot{\rho}_{\text{b}} = A_{\text{b}}(S) H(\phi) \quad (17)$$

$$\dot{\rho}_{\text{m}} = A_{\text{m}}(S) H(\phi) \quad (18)$$

In the remodeling evolution rules, A_{b} and A_{m} account for different phenomena of biological and mechanical nature together with some geometrical circumstances: i) the surface available for resorption or synthesis ‘‘inside’’ the considered material particle depends, as already discussed, on the ‘‘effective’’ porosity field, ii) the different properties of bone tissue and bio-material determine different resorption rates, due to the different effect of actor cells on these different material, iii) the rate of synthesis of bone tissue which is consequence of a positive stimulus is different from the resorption rate determined by a negative stimulus of the same amount. The previous considerations are consequence of the biological nature of the process of synthesis and resorption: in particular osteoclasts resorb at the same time both the bone-tissue and the resorbable

material while osteoblasts produce only bone tissue. In particular, the following forms for the functions H , A_b and A_m have been chosen to perform numerical simulations:

$$H = k\phi(1 - \phi) \quad (19)$$

$$A_b(S) = \begin{cases} s_b S & \text{for } S \geq 0 \\ r_b S & \text{for } S < 0 \end{cases} \quad (20)$$

$$A_m(S) = \begin{cases} 0 & \text{for } S \geq 0 \\ r_m S & \text{for } S < 0 \end{cases} \quad (21)$$

where the functions A_b and A_m are piece-wise linear functions with different slopes for negative and positive values of stimulus. For the bio-material and positive values of the stimulus, A_m must vanish, as there cannot be synthesis of bio-material, and the function H is designed in order to account for the influence of “effective” porosity on the biological activity of actor cells: when “effective” porosity is too large there is not enough material on which actor cells may deposit, when it is too small there is not enough free space in the pores to allow their mobility and deposit. We choose the shape of H in such a way that $H = 0$ for $\phi = 0$ or $\phi = 1$; s_b and r_b will be called synthesis rate and resorption rate for bone tissue respectively and r_m will be called resorption rate for bio-material; k is a suitable constant parameter, which was assumed equal to 4 in the performed numerical simulations. A characteristic time t_{ref} can be interpreted as the order of magnitude (months) of the time duration in which the physiological processes that lead to fulfilment of the phenomenon of material resorption and bone synthesis are accomplished. Dividing Eqs. (17) and (18) by ρ_{Max} , introducing the dimensionless time $\tilde{t} = t/t_{\text{ref}}$ and considering the constitutive assumptions, Eqs. (20) and (21) their dimensionless form reads:

$$\frac{\partial \rho_b}{\partial t} = \frac{\partial (\tilde{\rho}_b \rho_{\text{Max}})}{\partial (\tilde{t} t_{\text{ref}})} = \frac{\rho_{\text{Max}}}{t_{\text{ref}}} \frac{\partial (\tilde{\rho}_b)}{\partial (\tilde{t})} = \frac{\rho_{\text{Max}}}{t_{\text{ref}}} \dot{\tilde{\rho}}_b = A_b(\tilde{S} P_{\text{ref}}) H(\phi) \quad (22)$$

$$\frac{\partial \rho_m}{\partial t} = \frac{\partial (\tilde{\rho}_m \rho_{\text{Max}})}{\partial (\tilde{t} t_{\text{ref}})} = \frac{\rho_{\text{Max}}}{t_{\text{ref}}} \frac{\partial (\tilde{\rho}_m)}{\partial (\tilde{t})} = \frac{\rho_{\text{Max}}}{t_{\text{ref}}} \dot{\tilde{\rho}}_m = A_m(\tilde{S} P_{\text{ref}}) H(\phi) \quad (23)$$

$$\dot{\tilde{\rho}}_b = \frac{t_{\text{ref}}}{\rho_{\text{Max}}} \begin{cases} s_b \tilde{S} P_{\text{ref}} & \text{for } \tilde{S} P_{\text{ref}} \geq 0 \\ r_b \tilde{S} P_{\text{ref}} & \text{for } \tilde{S} P_{\text{ref}} < 0 \end{cases} = \frac{t_{\text{ref}}}{\rho_{\text{Max}}} P_{\text{ref}} \begin{cases} s_b \tilde{S} & \text{for } \tilde{S} \geq 0 \\ r_b \tilde{S} & \text{for } \tilde{S} < 0 \end{cases} = \begin{cases} \tilde{s}_b \tilde{S} & \text{for } \tilde{S} \geq 0 \\ \tilde{r}_b \tilde{S} & \text{for } \tilde{S} < 0 \end{cases} \quad (24)$$

where $\tilde{s}_b = s_b \frac{t_{\text{ref}}}{\rho_{\text{Max}}} P_{\text{ref}}$ and $\tilde{r}_b = r_b \frac{t_{\text{ref}}}{\rho_{\text{Max}}} P_{\text{ref}}$

$$\dot{\tilde{\rho}}_m = \frac{t_{\text{ref}}}{\rho_{\text{Max}}} \begin{cases} 0 & \text{for } \tilde{S} P_{\text{ref}} \geq 0 \\ r_m \tilde{S} P_{\text{ref}} & \text{for } \tilde{S} P_{\text{ref}} < 0 \end{cases} = \frac{t_{\text{ref}}}{\rho_{\text{Max}}} P_{\text{ref}} \begin{cases} 0 & \text{for } \tilde{S} \geq 0 \\ r_m \tilde{S} & \text{for } \tilde{S} < 0 \end{cases} = \begin{cases} 0 & \text{for } \tilde{S} \geq 0 \\ \tilde{r}_m \tilde{S} & \text{for } \tilde{S} < 0 \end{cases} \quad (25)$$

where $\tilde{r}_m = r_m \frac{t_{\text{ref}}}{\rho_{\text{Max}}} P_{\text{ref}}$.

It should be admitted that the choice of parameters used in our model was partially dictated by a necessity of future identification and a nature of biological effects considered in this work.

2.6 Geometrical and mechanical properties of sample

The following common values were assumed to characterize the geometrical and mechanical properties of the sample: $L_b = L_m = 1.25$ mm, $H_b = H_m = 1.00$ mm, $\rho_{b\text{Max}} = \rho_{m\text{Max}} = 1800$ kg/m³, $Y_{b\text{Max}} = Y_{m\text{Max}} = 18$ GPa, $\nu = 0.3$, $\varepsilon_{\text{ref}} = 1000$ $\mu\text{strain} = 0.001 = 0.1\%$, $s_b = 1.0$, $r_b = 1.0$, $r_m = 0.50$,

The influence distance $D = L/10$ was assumed equal to the thickness of five layers of osteocytes from the bone surface (and micro-venues). In order to consider a potential mesh refinement we should determine the size of the smallest region of influence which fits the biological behavior. Thus, the mesh size was chosen as a suitable fraction ($1/4$) of the influence distance D , to accomplish a numerical integration sufficiently accurate for the problem at hand. Time duration is equal to 0.15 time units. At the beginning of the process ($t = 0$), the initial values of mass densities were assumed to be $\rho_{b0} = \rho_{m0} = 900$ kg/m³, and therefore Young’s moduli, according to Eq. (3), became: $Y_{b0} = Y_{m0} = 4.5$ GPa.

3 Results

The study presented here is of theoretical nature and is focused in explanation and better understanding of possible effects and their dependence on different parameters. The proposed model needs future identification of defined parameters in order to perform its validation in different characteristic situations. However the effects observed in numerical calculations discussed in the present paper were already reported by orthopedic surgeons active in clinical practice. Additional important goal was providing tools useful in planning future experimental tests.

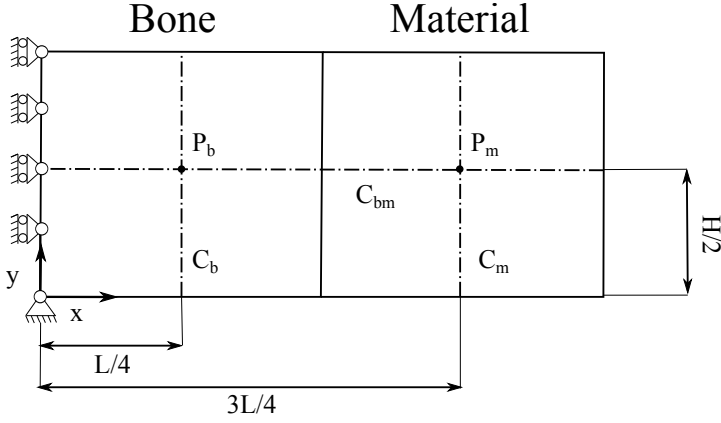


Fig. 2 Details of schematic computational 2D model shown in Fig. 1, with indicated sub-domains where different parameters are defined and results are presented.

Table 1 Values of the parameters used in numerical simulations.

$\tilde{\rho}_{b0}$	$\tilde{\rho}_{m0}$	\tilde{Y}_{bMax}	\tilde{Y}_{mMax}	k	θ	\tilde{s}_b	\tilde{r}_b	\tilde{r}_m	$\beta_b = \beta_m$	η	\tilde{D}	$P_{ref} [J]$
0.5	0.5	1.0	1.0	4	1	3.47×10^4	3.47×10^4	1.74×10^4	2.0	1.0	0.1	3.47×10^{-4}

3.1 Generalities

In order to show that the presented model is able to describe different possible mechanisms of bone remodeling among those induced by the presence of bio-material a simple 2-D problem will be studied which seems to be the simplest possible presenting some of the required complex features of the formulated model. In order to simplify the study of the mechanical part of the problem, a sample is considered which behaves as a membrane (composed by two materials) with variable (with respect to time and space) elastic modulus and porosity. The sequence of configurations of the considered bone-material sample were calculated via *COMSOL Multiphysics*, where a discrete time step increment algorithm is implemented. The case of a 2D membrane sample is considered of length L with initially completely separated bone tissue and bio-material, thus assuming that one part of the slab is initially occupied by pure bone tissue and the remaining part is occupied by pure bio-material. The slab is clamped at $x = 0$ ($u(0, y, t) = 0, v(0, 0, t) = 0 \forall t$) and is loaded by a static traction f_x at $x = L$, Fig. 1; the homeostatic strain state (see Subsect. 2.4) ε_{ref} was obtained in average by assuming $Y_{b0} = Y_{m0} = Y_{Max}/4$, Eq. (3), $\nu = 0.3$, and applying a traction of 14.2 MPa; this value was assumed as the reference value f_{xref} to normalizing the external load $\tilde{f}_x = f_x/f_{xref}$. In Figure 2, C_{bm} is the longitudinal Cauchy cut in the whole domain, C_b is the transversal Cauchy cut in the bone zone, C_m is the transversal Cauchy cut in the material zone, P_b is the probe point in the bone zone, and P_m is the probe point in the material zone. As far the sizes of the specimen were concerned, it is assumed that $L = L_b + L_m$, $H = H_b = H_m$, and the ratio $H/L = 0.4$. The sampling lines and points are indicated in Fig. 2.

The values assigned to the governing parameters in the performed numerical simulations are reported in Table 1.

The length L of the specimen was chosen as characteristic length scale, while the parameter D was assumed equal to $L/10$ in the performed numerical simulations. The influence of the parameters governing the proposed model will be studied referring to global synthesis and resorption phenomena in space and time. The aim of the analysis is to explain and discuss the variety of phenomena which may occur depending on the different mechanical, geometrical and biological properties of used bio-materials and their placement in the grafted bone. In particular, the biological and mechanical properties of the composite material which is finally resulting from surgical bone reconstruction will be considered, after the complete healing and remodeling process. The performed analyses should give an indication about how the bio-material should be used in bone reconstruction. The three following examples are characterized by different values of the non-dimensional load \tilde{f}_x applied on the right boundary (the left being fixed): 1.0 (Subsect. 3.2), 2.6 (Subsect. 3.3), 3.16 (Subsect. 3.4), 6.32 (Subsect. 3.5). The Case $\tilde{f}_x = 2.6$ was studied when the influence function is an absolute exponential function (Eq. (14)), and a quadratic exponential function of distance (Eq. (15)). In Subsect. 3.6 a parametric analysis was worked out by varying some key parameters, namely resorption rate of resorbable bio-material (\tilde{r}_m), non-dimensional external load (\tilde{f}_x), and homeostatic deformation (ε_{ref}) of living bone tissue, within suitable ranges.

3.2 Homeostatic Case

The first case which was analyzed was characterized by a non-dimensional traction $\tilde{f}_x = 1.0$, which corresponds to an initial homeostatic deformation state (see 3.1). Figure 3 shows the three-dimensional representation of two-dimensional final distribution of mass densities of bone (a) and material (b) in the whole domain at the end of the process.

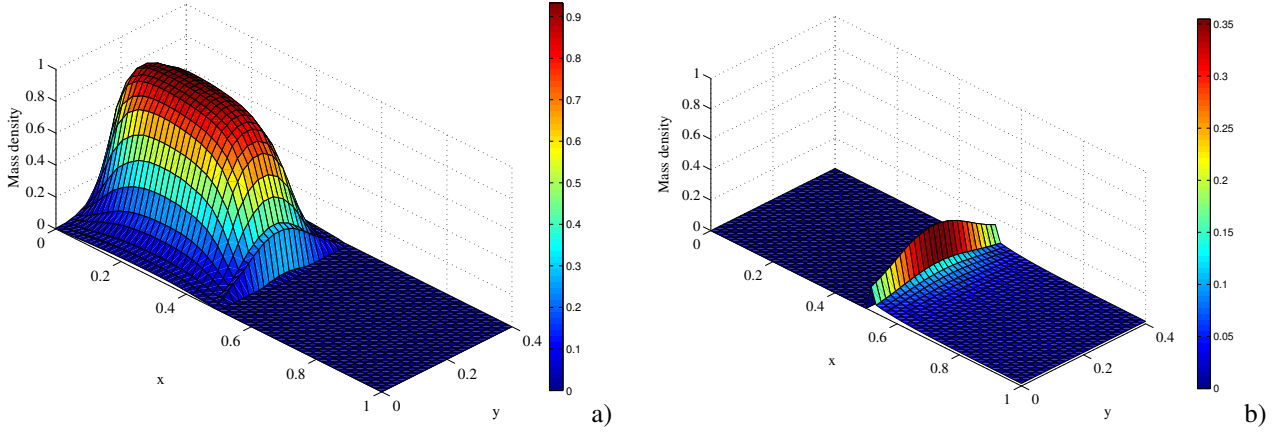


Fig. 3 3D representation of 2-dimensional final distribution of mass densities of bone (a) and material (b).

Observing Figure 3a, it can be noted that the bone does not reach saturation. In fact, the analysis was stopped as soon as the material has been entirely resorbed, since in this situation is no longer possible to transmit the load to the structure. In fact a small amount of material has remained at the interface ($\rho_m \neq 0$), as can be seen by observing Fig. 3b; in such a way the continuity of the mass density ρ of the mixture is maintained. Another observation that can be done regards the non-uniformity of the distribution of the mass density of the bone. On one hand, it is true that the load was evaluated according to a homeostatic state of uniform deformation, but on the other hand the stimulus is a function of the point and hence ρ_b is not conserved uniform, reflecting the distribution of the stimulus and the edge effects. In this regard, it is interesting to compare the distribution of ρ_b shown in Fig. 3a with that of S , given by Eq. (13) and represented in Fig. 4, which shows the distribution of the non-dimensional mechanical stimulus in the whole domain at the end of the process.

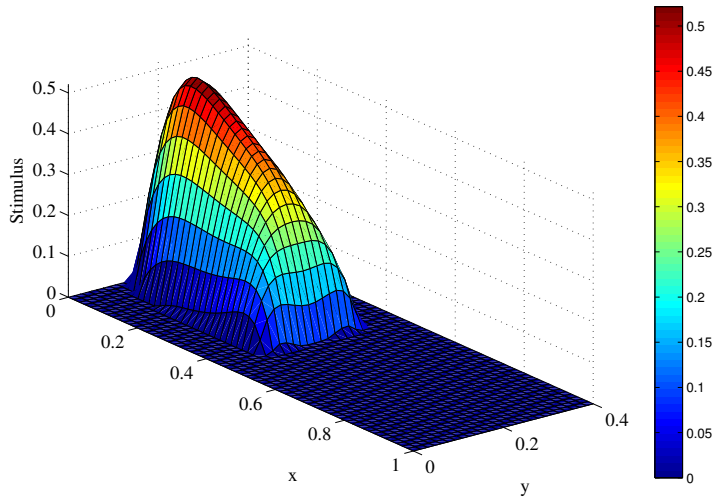


Fig. 4 3D representation of 2-dimensional final distribution of the stimulus.

Figure 5 shows the evolutions in time of mass densities of bone in the probe point P_b (a) and of bone and material in the probe point P_m (b). The process was interrupted due continuity loss of material.

With reference to Figure 5a, at the beginning changes happen very slowly due to the fact that a situation homeostatic is being analysed, in the sense that the strain energy initially stored in the sample is approximately uniform and equal to the homeostatic value. Then the balance is lost due to the unevenness caused by the stimulus.

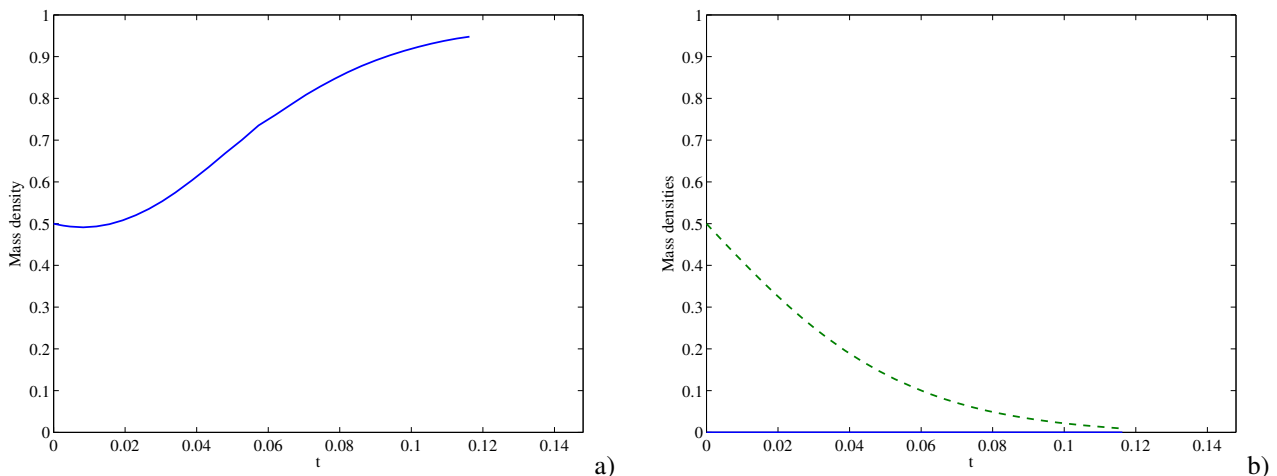


Fig. 5 Time evolutions of mass densities of bone in P_b (a) and of bone (solid line) and material (dashed line) in P_m (b).

3.3 Minimum applicable load

3.3.1 Influence distance via absolute exponential function

This case (denoted Case 1a, from this point on) was characterized by accounting for the influence distance by means of the absolute exponential function of Eq. (14) and by applying a non-dimensional traction $\tilde{f}_x = 2.6$. This value represents a threshold below which the material continuity is lost at $x = L$ and hence the external load cannot be longer transmitted to the sample. The phenomenon can be described to take place through the following steps. The bone arrives at saturation in the bone zone, beginning to penetrate in the material zone, while at the same time the material is resorbed. At this point the bone complete its penetration in the material zone, reaching a value close to the maximum density at the region of load application, where the stimulus is highest and where the mixture saturates ($\rho = \rho_{\text{Max}}$). The rate of remodelling is dependent of the signal from sensor cells and porosity of the material. So the final effect depends to much extent on the ratio between the resorption of the material and the synthesis of the tissue. The stimulus is larger in the regions close to the domains of large osteocytes density, that is in the places where we observe large contribution of tissue in a composite (closer to left sub-domain). On the other hand the remodelling rate is also controlled by a number of actor cells which is dependent on porosity. Therefore there exists a game between these effects and in some situations the “incorrect” porosity may slow down synthesis in spite of large signal from osteocytes or opposite – optimal porosity support fast synthesis in spite of moderate stimulus. As a result of this effects one can observe at the right-hand edge in some situations creation of void or a composite tissue-graft and sometimes replacement of a graft by a tissue. The crucial aspects that characterize this phenomenon are (i) the synthesis of the bone until saturation in the bone zone and its spread in the material zone, and (ii) the resorption of the material, that, if it is too fast, does not give time to the bone to replace it and lose continuity to the structure, preventing the transmission of the load. Figure 6 shows the two-dimensional distributions of mass densities of bone (a) and material (b) in the whole domain at the end of the process; a diffusion-like process led the bone tissue to spread inside the material zone.

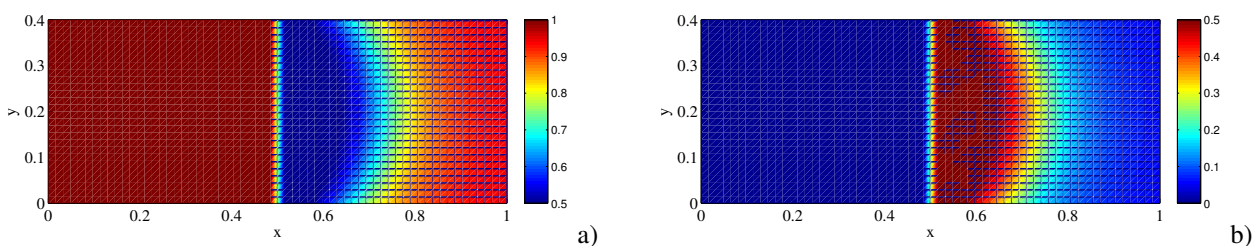


Fig. 6 2-D final distributions of mass densities of bone (a) and material (b).

Figures 7 show the one-dimensional distributions of mass densities of bone and material at the longitudinal Cauchy cut C_{bm} (a) and at the transversal Cauchy cut C_m (b) at the end of the process. Saturation of mass density of bone tissue occurred in the bone zone, whereas the bio-material was almost completely resorbed and substituted by bone tissue at the right hand side of the material zone, near the zone of load application.

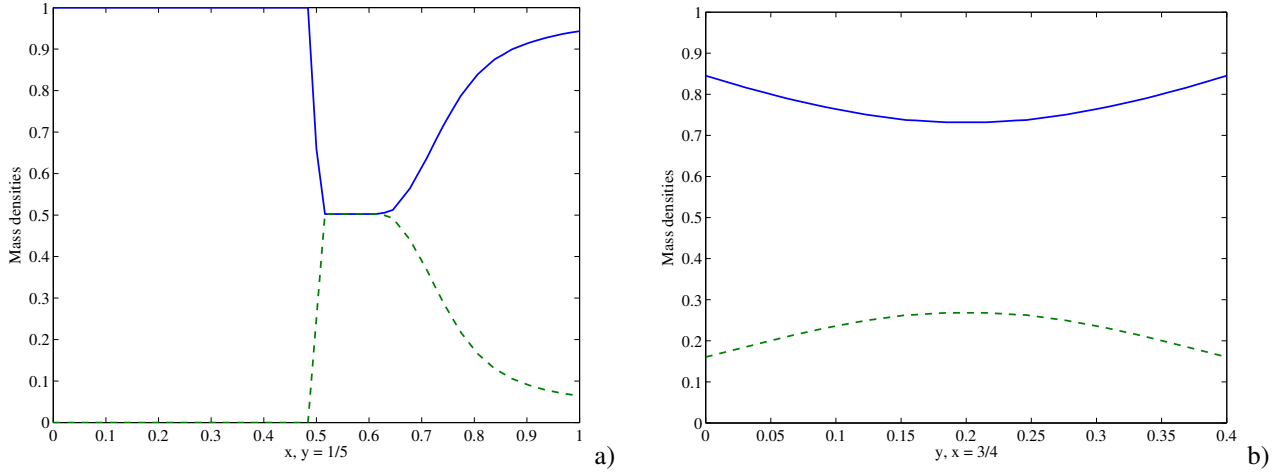


Fig. 7 1-D final distributions of mass densities (solid line, bone; dashed line, material) along C_{bm} (a) and C_m (b).

Mass density of bone tissue saturated at $\rho = \rho_{Max}$ in the bone zone; therefore its final one-dimensional distribution along the transversal Cauchy cut C_b was not shown. Figure 8 shows the three-dimensional representation of two-dimensional final distribution of mass densities of bone (a) and material (b) in the whole domain at the end of the process.

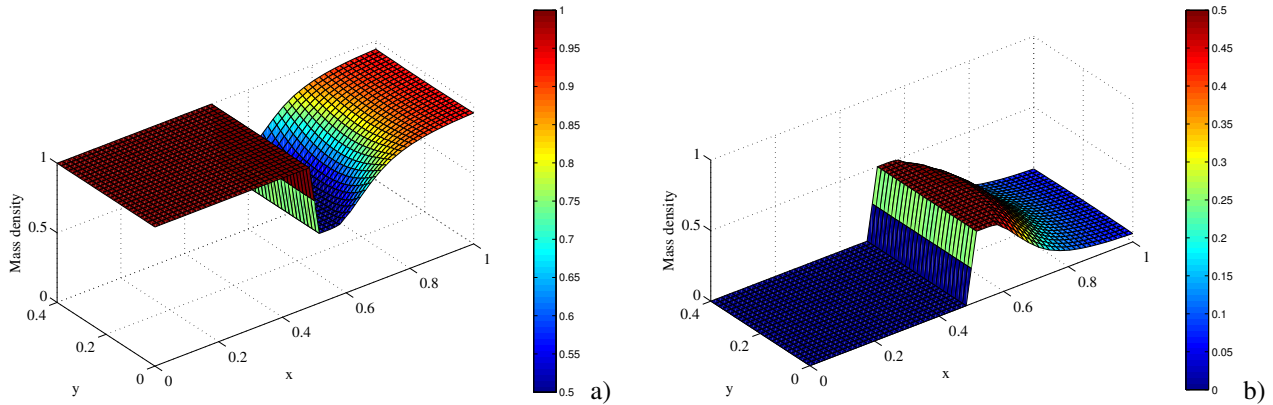


Fig. 8 3D representation of 2-dimensional final distribution of mass densities of bone (a) and material (b).

Looking at Fig. 8 it can be noted that the continuity of the mixture is preserved throughout, ensuring the transmission of external force to the structure. Figure 9 shows the distribution of the non-dimensional mechanical stimulus in the whole domain at the end of the process.

Figure 10 shows the evolutions in time of mass densities of bone in the probe point P_b (a) and of bone and material in the probe point P_m (b).

From Figs. 10a and 10b one can see that the rate of growth of the bone is visibly greater than that of the resorption of the material, consistent with the data assigned in Subsect. 3.1. It can also be observed that the growth of the bone begins after the stabilization of the material, at least in the probe point selected. In the bone zone, bone rapidly grew up to saturation; in the material zone, material slowly resorbed, while bone formed at high speed after material attained a constant value of mass density; an asymptotic behaviour was exhibited in any case.

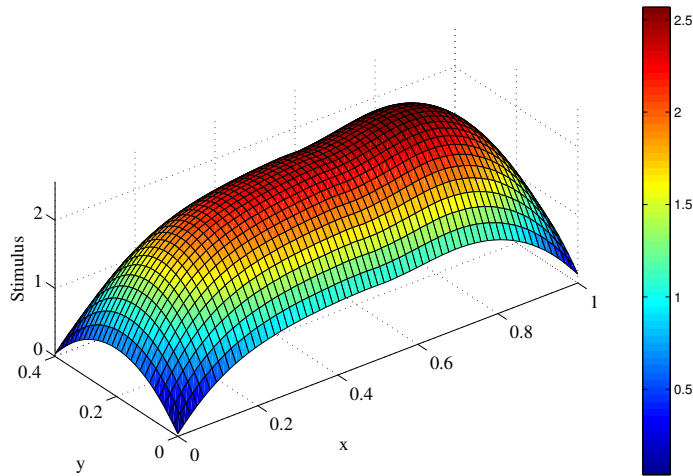


Fig. 9 3D representation of 2-dimensional final distribution of the stimulus.

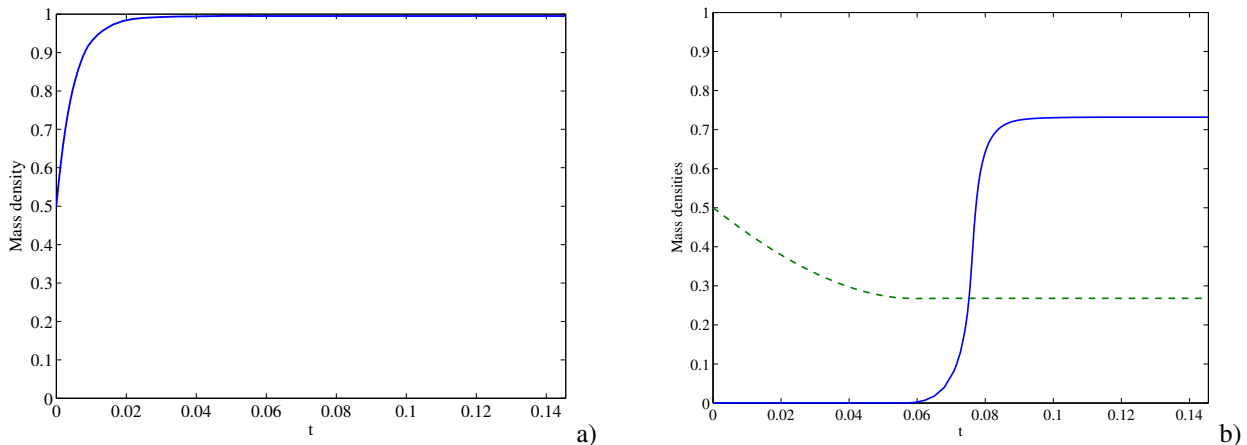


Fig. 10 Time evolutions of mass densities of bone in P_b (a) and of bone (solid line) and material (dashed line) in P_m (b).

3.3.2 Influence distance via quadratic exponential function

This case (denoted Case 1b, from this point on) was characterized by accounting for the influence distance by means of the quadratic exponential function of Eq. (15) and by applying (as in Case 1a) a non-dimensional traction $\tilde{f}_x = 2.6$. For Case 1b the same considerations can be done which have been presented at the beginning of the previous Subsect. 3.3.1 relative to the Case 1a. Figure 11 shows the two-dimensional distributions of mass densities of bone (a) and material (b) in the whole domain at the end of the process.

Figures 12 show the one-dimensional distributions of mass densities of bone and material at the longitudinal Cauchy cut C_{bm} (a) and at the transversal Cauchy cut C_m (b) at the end of the process.

Figure 13 shows the three-dimensional representation of two-dimensional final distribution of mass densities of bone (a) and material (b) in the whole domain at the end of the process. The results relative to the Cauchy cut C_b were not shown because trivial.

Figure 14 shows the distribution of the non-dimensional mechanical stimulus in the whole domain at the end of the process.

Figure 15 shows the evolutions in time of mass densities of bone in the probe point P_b (a) and of bone and material in the probe point P_m (b). From Figure 15b it can be inferred that the bone begins to form as soon as the material has reached a constant mass density, at least in the probe point selected.

Looking at Fig. 10b it can be noted that, at the end of the analysis, the continuity of the mixture is preserved throughout, ensuring the transmission of external force to the structure. However, we cannot exclude a priori the possibility that all throughout the analysis the material undergoes a local damage. In some situations, the damage may be so extensive as to

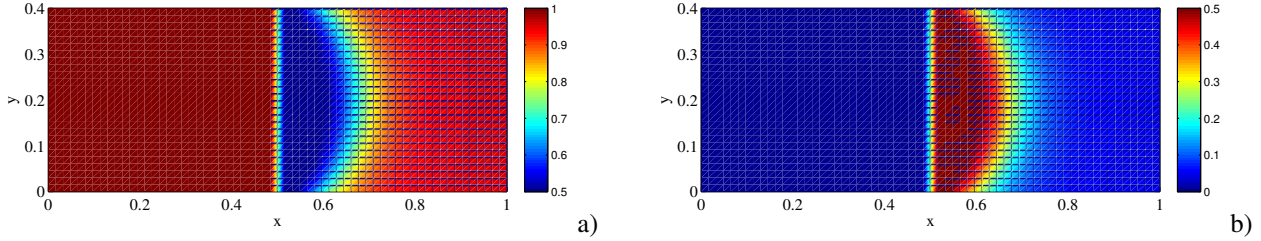


Fig. 11 2-D final distributions of mass densities of bone (a) and material (b).

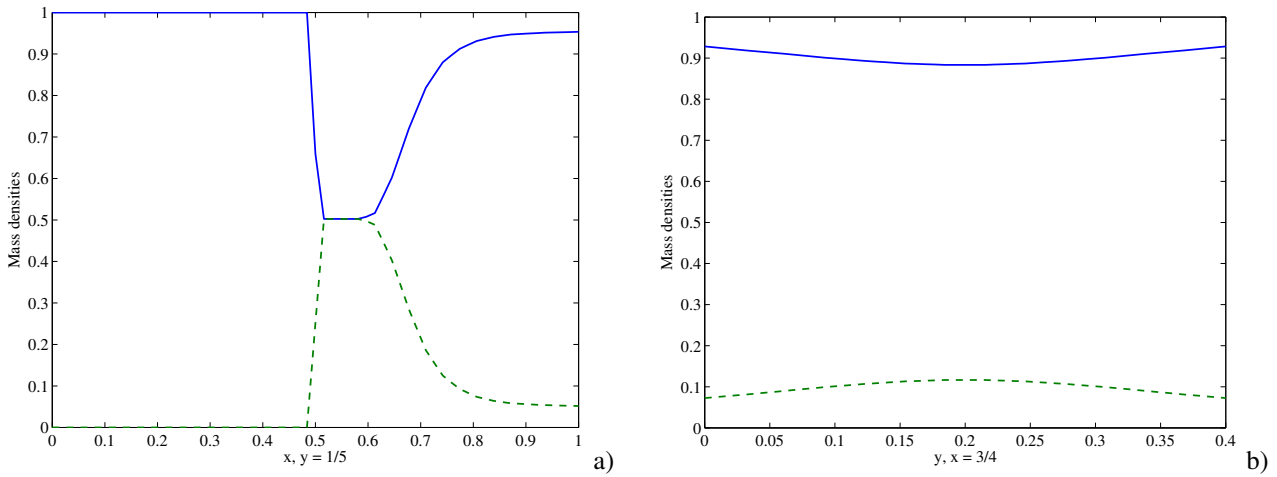


Fig. 12 1-D final distributions of mass densities (solid line, bone; dashed line, material) along C_{bm} (a) and C_m (b).

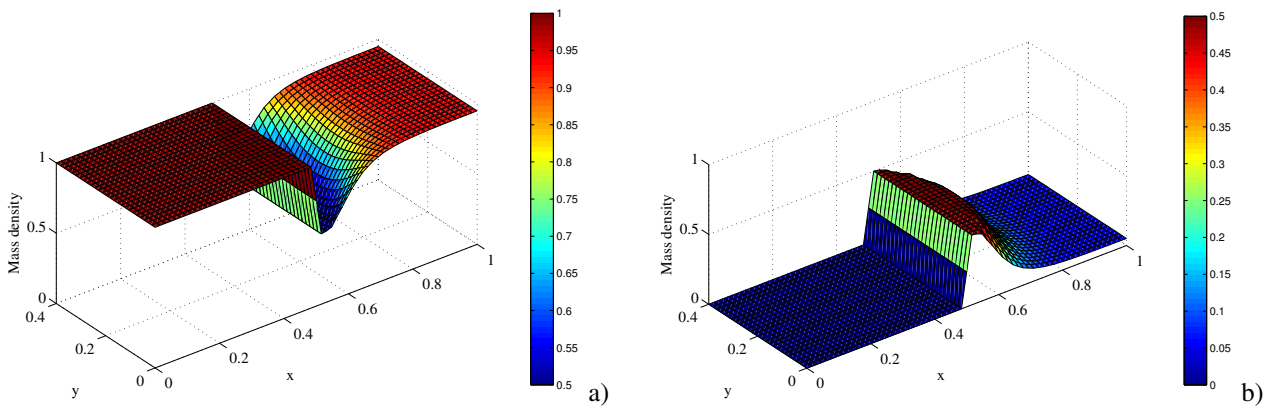


Fig. 13 3D representation of 2-dimensional final distribution of mass densities of bone (a) and material (b).

affect the possibility of transmission of external load to the structure. In other situations, the damage can be confined to small areas and the load can be transferred to other coexisting parts of the structure remained still intact, that contribute to endure it. In such cases it should be noted the usefulness of the two-dimensional model, which allows to take into account the availability of areas not damaged. For comparison's sake, in Fig. 15b it can be observed that the time range before bone starts to regenerate is much shorter with respect to that one exhibited in Fig. 10b; it in fact depends on the time instant when

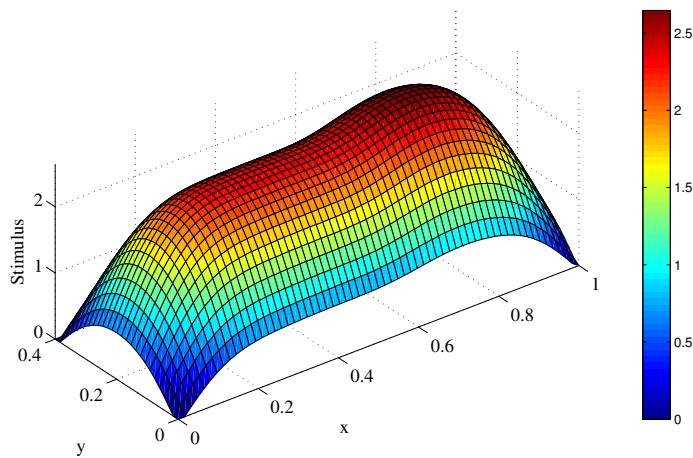


Fig. 14 3D representation of 2-dimensional final distribution of the stimulus.

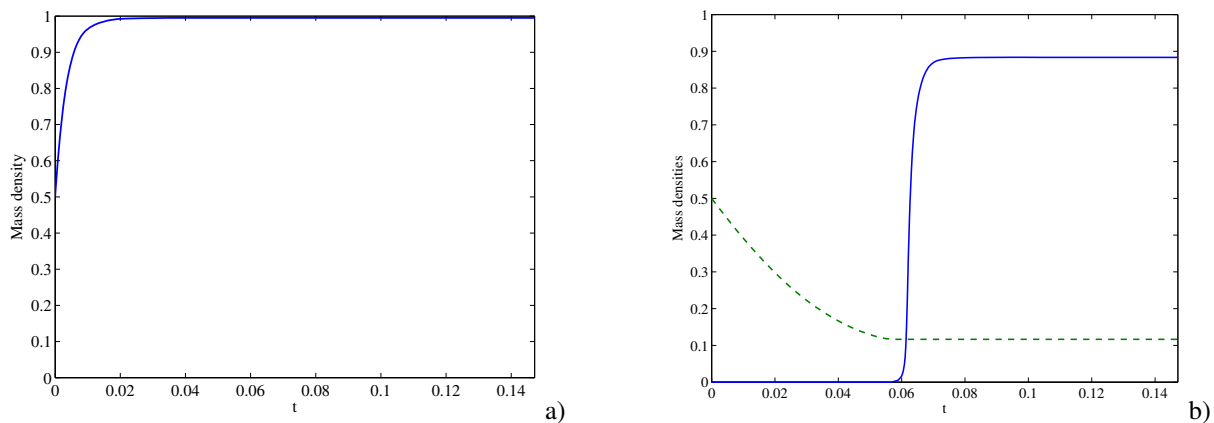


Fig. 15 Time evolutions of mass densities of bone in P_b (a) and of bone (solid line) and material (dashed line) in P_m (b).

the bone starts to be formed and by the rate of growth of bone; these quantities can be in turn controlled by an appropriate choice of parameters characterizing material and loading.

3.3.3 Comparison between absolute exponential function and quadratic exponential function

Figure 16 shows the comparison between the cases presented in Subsections 3.3.1 (Case 1a) and 3.3.2 (Case 1b) as far as the one-dimensional distributions of mass densities along the longitudinal Cauchy cut C_{bm} (a) and along the transversal Cauchy cut C_m (b) are concerned.

Figure 17 shows the comparison between Cases 1a and 1b as far as the time evolutions of mass densities of bone in the probe point P_b (a) and of bone and material in the probe point P_m (b) are concerned.

With reference to Fig. 17b, it can be seen that the instant at which the material reaches a constant value of mass density and the bone begins to form at the probe point, does not depend on the type of function used to take into account the influence distance. The quadratic exponential function weighs more points close and so reinforces the stimulus with respect to the absolute exponential function, and therefore in Case 1b the formation of bone takes place at greater rate and smaller delay with respect to the Case 1a, reaching a higher density.

3.4 Intermediate value of the applied load

A non-dimensional traction $\tilde{f}_x = 3.16$ was applied in this case. The bone saturated in the bone zone and grew up in the material zone, where the material partially resorbed. Figure 18 shows the two-dimensional distributions of mass densities of bone (a) and material (b) in the whole domain at the end of the process.

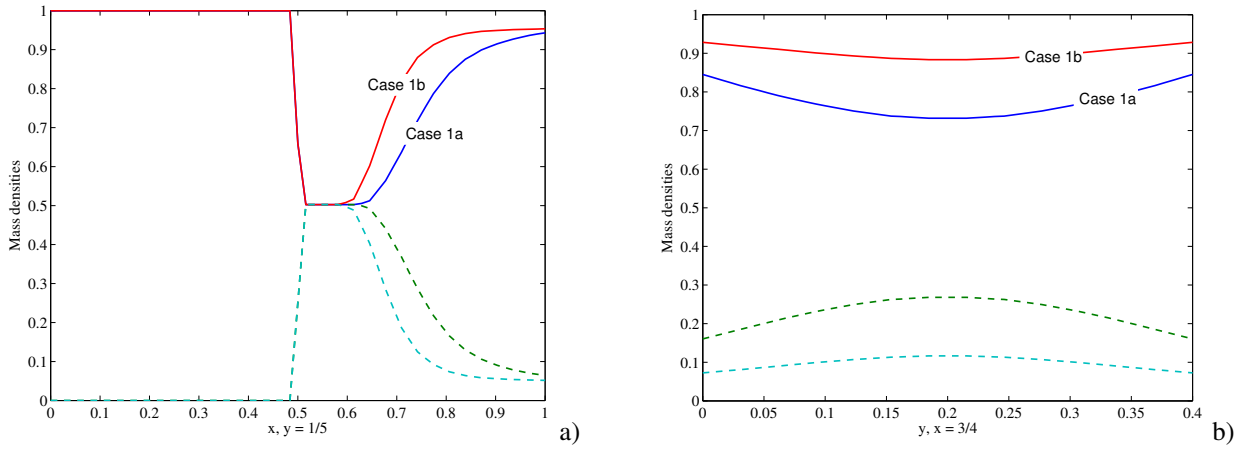


Fig. 16 1-D final distributions of mass densities (solid line, bone; dashed line, material) along C_{bm} (a) and C_m (b).

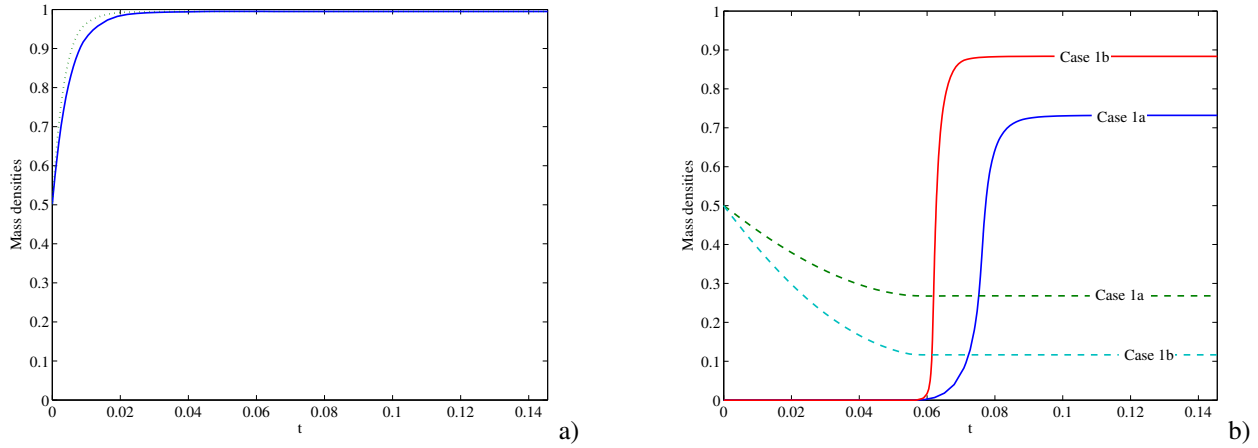


Fig. 17 Time evolutions of mass densities of bone in P_b (solid line, Case 1a; dotted line, Case 1b) (a) and of bone (solid line) and material (dashed line) in P_m (b).

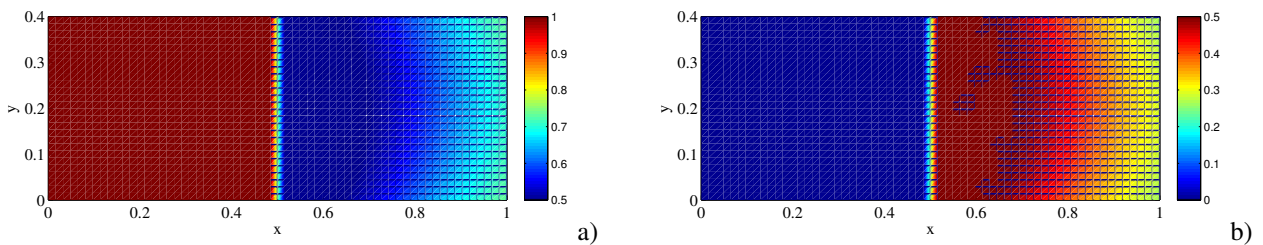


Fig. 18 2-D final distributions of mass densities of bone (a) and material (b).

Figures 19 show the one-dimensional distributions of mass densities of bone and material at the longitudinal Cauchy cut C_{bm} (a) and at the transversal Cauchy cut C_m (b) at the end of the process.

Figure 20 shows the three-dimensional representation of two-dimensional final distribution of mass densities of bone (a) and material (b) in the whole domain at the end of the process.

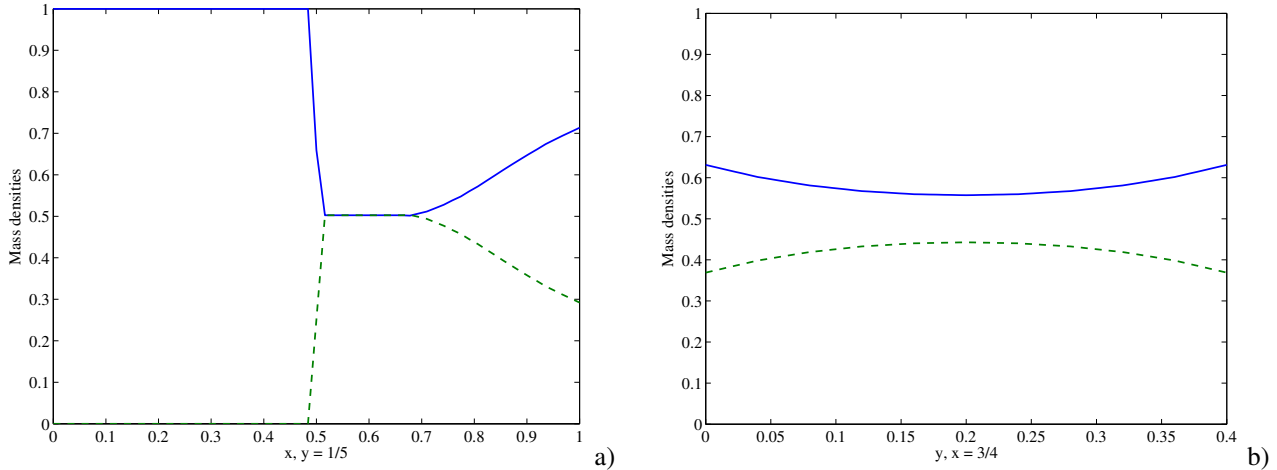


Fig. 19 1-D final distributions of mass densities (solid line, bone; dashed line, material) along C_{bm} (a) and C_m (b).

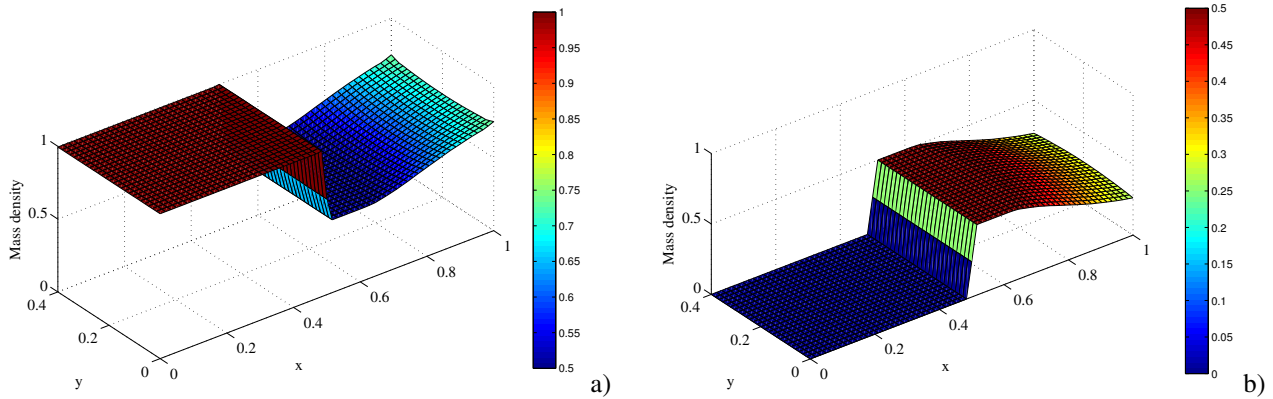


Fig. 20 3D representation of 2-dimensional final distribution of mass densities of bone (a) and material (b).

From Figs. 19 and 20 one can draw an indication that this case is similar to the Case 1a of Subject. 3.3.1, with the difference that load being higher, the bone saturated sooner and invades sooner the material zone and therefore does not leave time sufficient for the material to be resorbed; in fact, ρ_m is greater with respect to the Case 1a. Figure 21 shows the distribution of the non-dimensional mechanical stimulus in the whole domain at the end of the process.

From Fig. 21 it is noted that the stimulus is significantly increased compared to Case 1a, while retaining a similar shape, as it is increased the load. Figure 22 shows the evolutions in time of mass densities of bone in the probe point P_b (a) and of bone and material in the probe point P_m (b).

Also in this case it is evident (at least at the probe point) that the formation of bone begins when the material is stabilized. The level of ρ_b (Fig. 22b) is smaller than that of the Case 1a (Fig. 10b), since the external force and therefore also the stimulus are greater, so the material resorbs less; therefore the bone finds less space free, having comply with the condition of the mixture $\rho = \rho_b + \rho_m \leq \rho_{Max}$.

The above depicted scenarios obviously depend on the given value of the P_{ref} parameter, as well as on the biological parameters used for bone growth and material resorption.

3.5 Maximum value of the applicable load

A non-dimensional traction $\tilde{f}_x = 6.8$ was applied in this case. The bone saturated in the bone zone and grew up in the material zone, where the material was unaffected by resorption due to the limit imposed by the mixture $\rho = \rho_b + \rho_m \leq \rho_{Max}$; therefore the relevant 2-D and 3-D distribution of mass densities of bone and material in the whole domain at the end of the process were not reported. Figures 23 show the one-dimensional distributions of mass densities of bone and material at the longitudinal Cauchy cut C_{bm} at the end of the process.

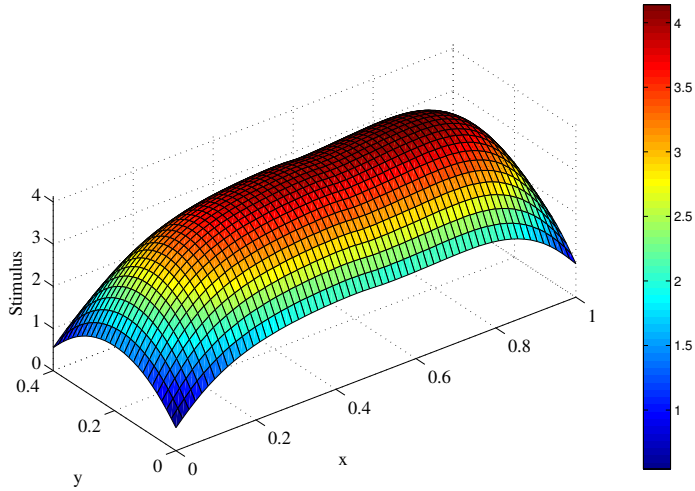


Fig. 21 3D representation of 2-dimensional final distribution of the stimulus.

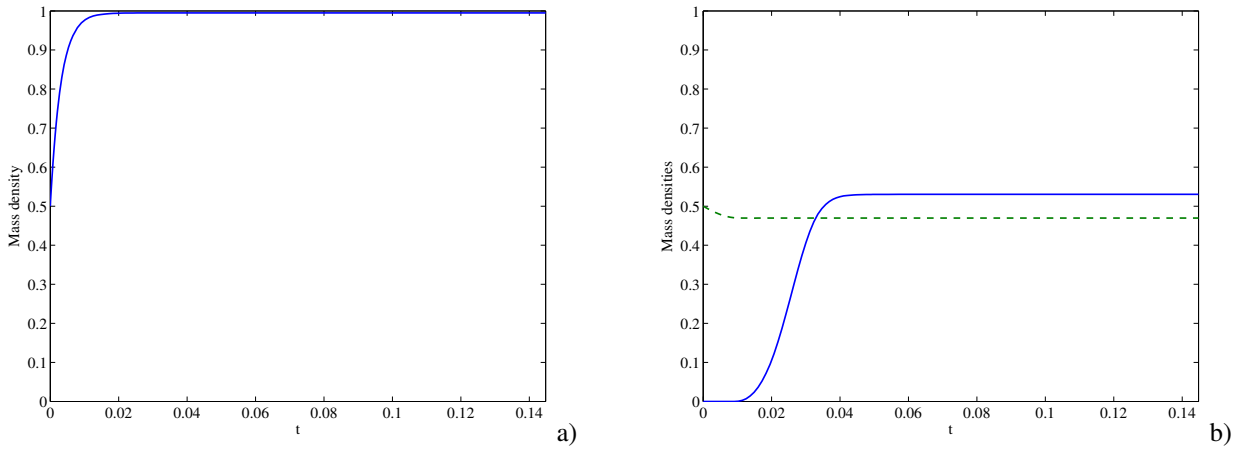


Fig. 22 Time evolutions of mass densities of bone in P_b (a) and of bone (solid line) and material (dashed line) in P_m (b).

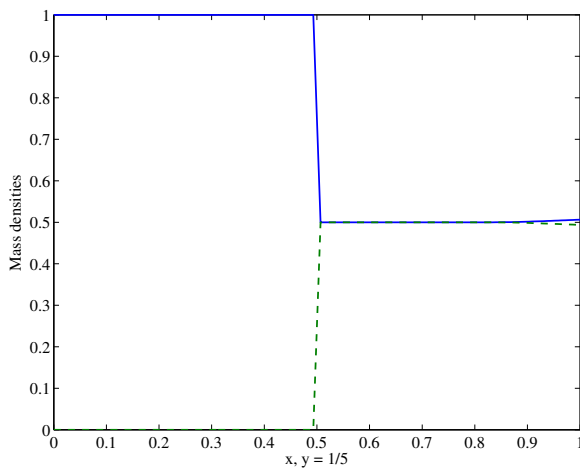


Fig. 23 1-D final distributions of mass densities of bone (solid line) and material (dashed line) along C_{bm} .

Mass density of bone tissue saturated at $\rho_b = \rho_{Max}$ in the bone zone, whereas it attained the initial value $\rho_b = \rho_{b0}$ in the material zone. It is worth to be noted that further increases of the load do not result in significant changes in the distributions depicted in Fig. 23. Therefore, the maximum value $\tilde{f}_x = 6.8$ should be interpreted in this sense.

Figure 24 shows the distribution of the non-dimensional mechanical stimulus in the whole domain at the end of the process.

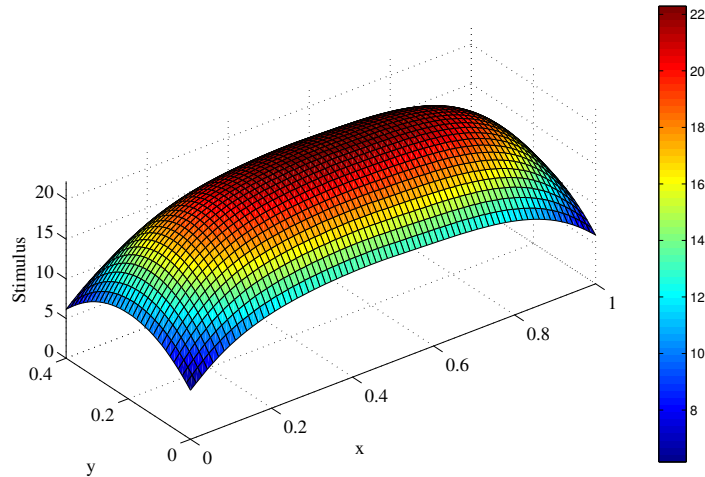


Fig. 24 3D representation of 2-dimensional final distribution of the stimulus.

The stimulus reaches a value much higher than in the previous cases, as a result of the load increment. Figure 25 shows the evolutions in time of mass densities of bone in the probe point P_b (a) and of bone and material in the probe point P_m (b).

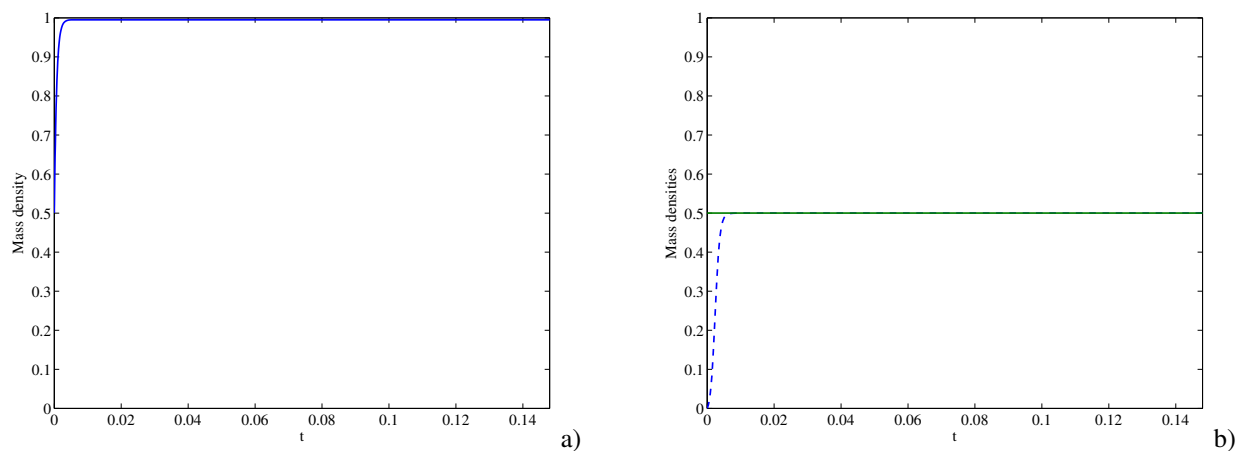


Fig. 25 Time evolutions of mass densities of bone in P_b (a) and of bone (dashed line) and material (solid line) in P_m (b).

The material does not undergo resorption (Fig. 25b), while the bone quickly saturated in the bone (Fig. 25a) and reaches the highest value of the mass density compatible with the mixture in the material.

3.6 Parametric analysis

The parametric analysis was performed by varying three parameters, namely, resorption rate of material \tilde{r}_m , applied load \tilde{f}_x , and homeostatic strain ε_{ref} .

3.6.1 Sensitivity to variations of the resorption rate of material

The resorption rate of the bio-resorbable material was varied within the range

$$\tilde{r}_m = 0.25 \times 3.47 \times 10^4 \div 2.5 \times 3.47 \times 10^4$$

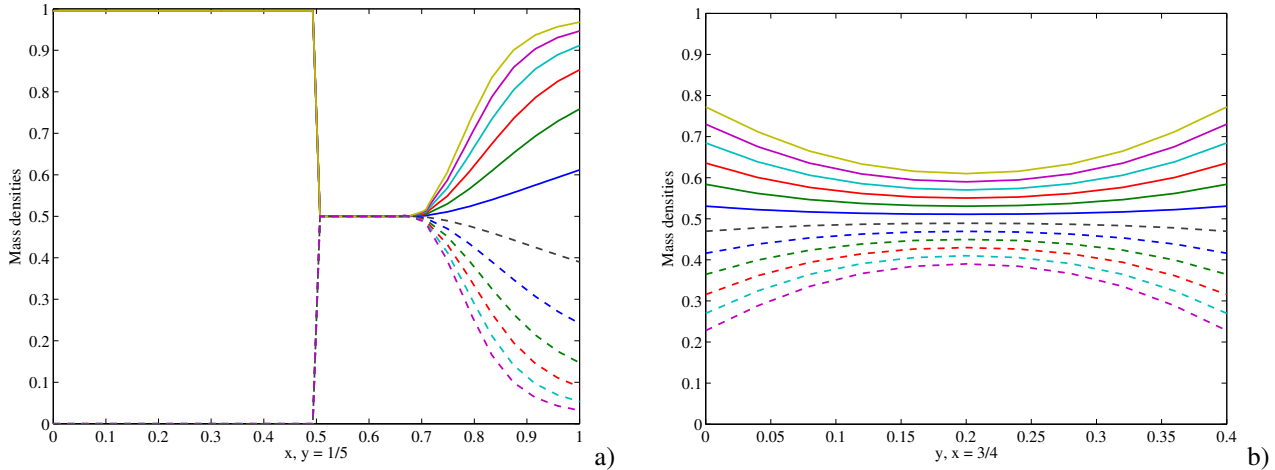


Fig. 26 1-D final distributions of mass densities of bone and material in Cauchy cuts (solid line, bone; dashed line, material) along C_{bm} (a) and C_m (b) – Sensitivity to variations of the resorption rate of material.

with a step 0.45. The applied load was $\tilde{f}_x = 3.16$ and the homeostatic strain was $\varepsilon_{ref} = 1000 \mu\text{strains}$.

In Fig. 26a, $\tilde{r}_m = 0.25 \times 3.47 \times 10^4$ corresponds to the “narrow fork” whereas $\tilde{r}_m = 2.5 \times 3.47 \times 10^4$ corresponds to the “wide fork”. In Fig. 26b the value of \tilde{r}_m increases as the plotted curves go far away from the middle line $\rho_b = \rho_m = 0.5$. With increasing rate \tilde{r}_m , the material is resorbed faster and in larger quantities and therefore there is more space for bone formation. This effect depends on values of the porosity ϕ , Eq. (12), that influence the evolution of the bone remodelling on the base of the shape of the parabola chosen to define the function H (see Eq. (19)); at the beginning of this computation the value of the porosity is equal to the optimum, *i.e.* 0.5, then the evolution proceeds to a worse situation moving away from the optimal initial one, namely $H = 1$. On the contrary, if the initial porosity is close to worse values, *i.e.* about zero or one, namely $H = 0$, the evolution proceeds to better values of porosity.

The distribution of bone mass density along the transversal cut C_b in the bone zone is not shown here because the bone saturated.

3.6.2 Sensitivity to variations of the applied load

The applied external load was varied within the range

$$\tilde{f}_x = 2.6 \div 6.8$$

with a step of 1.05. The resorption rate of material was $\tilde{r}_m = 0.5 \times 3.47 \times 10^4$ and the homeostatic strain was $\varepsilon_{ref} = 1000 \mu\text{strains}$. In Fig. 26a, $\tilde{f}_x = 6.8$ corresponds to the “narrow fork” whereas $\tilde{f}_x = 2.6$ corresponds to the “wide fork”. In Fig. 26b the value of \tilde{f}_x decreases very fast as the plotted curves go far away from the middle line $\rho_b = \rho_m = 0.5$. The greater the force \tilde{f}_x , the closer is the “fork”: the process of synthesis prevails over resorption.

3.6.3 Sensitivity to variations of the homeostatic strain

The homeostatic strain was varied within the range

$$\varepsilon_{ref} = 400 \div 1200 \mu\text{strains}$$

with a step 200. The resorption rate of material was $\tilde{r}_m = 0.5 \times 3.47 \times 10^4$ and the applied load was $\tilde{f}_x = 3.16$. In Fig. 28a, $\varepsilon_{ref} = 400$ corresponds to the “narrow fork” whereas $\varepsilon_{ref} = 1200$ corresponds to the “wide fork”. In Fig. 28b the value of ε_{ref} increases as the plotted curves go far away from the middle line $\rho_b = \rho_m = 0.5$.

The smaller the homeostatic deformation ε_{ref} , the tighter the fork and then the apposition prevails on the resorption.

4 Conclusions

In this paper a continuum model of a two-constituent mixture was used to describe the long-term growth/resorption phenomena in bone tissues grafted with bio-resorbable materials as driven by mechanical loads. This model has been formulated

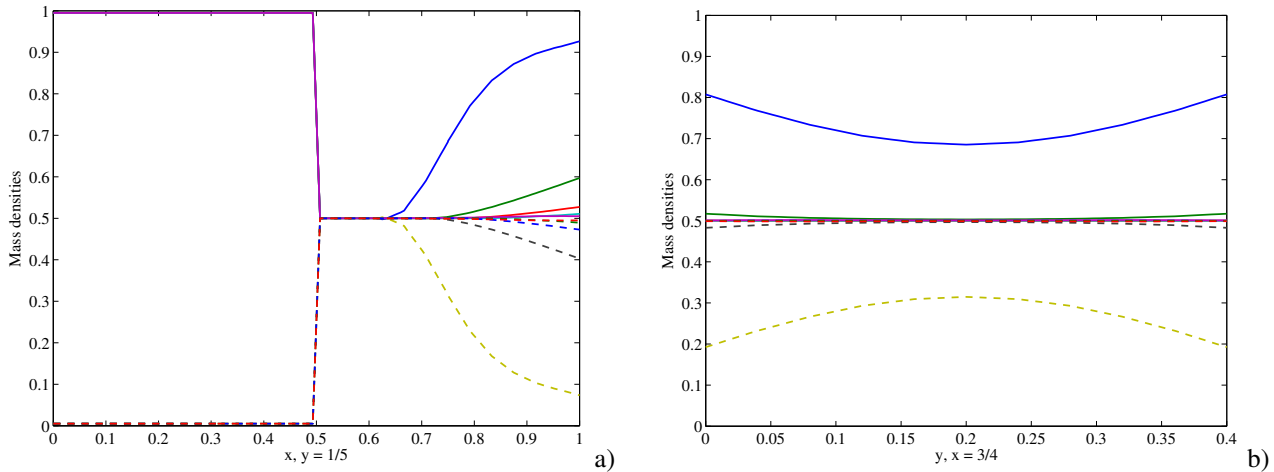


Fig. 27 1-D final distributions of mass densities of bone and material in Cauchy cuts (solid line, bone; dashed line, material) along C_{bm} (a) and C_m (b) – Sensitivity to variations of the applied load.

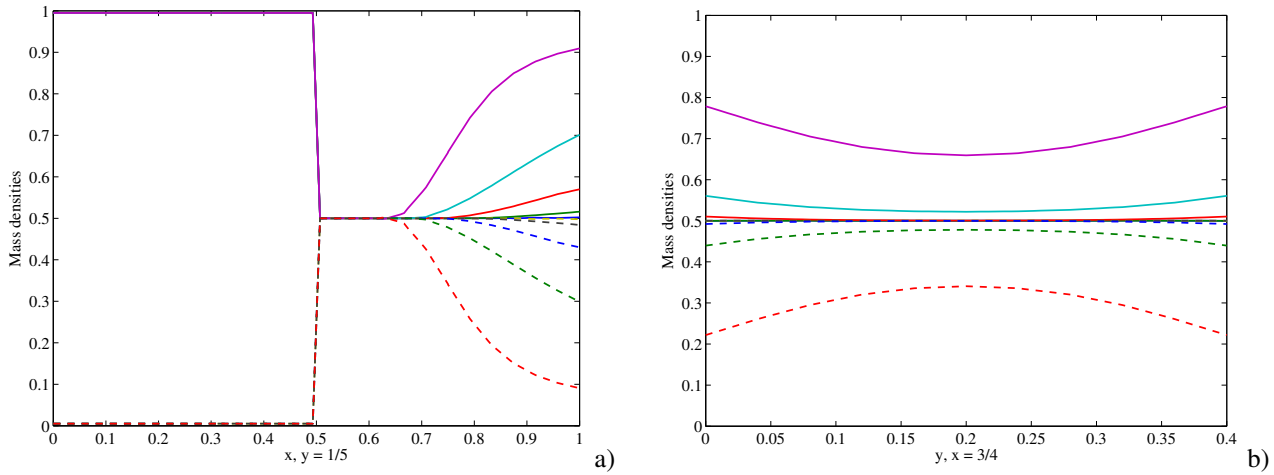


Fig. 28 1-D final distributions of mass densities of bone and material in Cauchy cuts (solid line, bone; dashed line, material) along C_{bm} (a) and C_m (b) – Sensitivity to variations of the homeostatic strain.

by [32, 36] considering the mixture as linear elastic; a 3D spatial model was presented and was used by them to work out numerical examples in 1D space. This model is able to account for the interaction between mechanical and biological phenomena which are known to be important for the bone tissue synthesis and the resorption of both bone tissue and bio-material. In particular, the Lagrangian apparent mass densities of the natural bone and of the artificial material evolve in time according to ordinary differential equations. These equations have been obtained by postulating growth/resorption laws and constitutive equations which account for the influence on bone resorption and synthesis of the action of different applied external loads as mediated by biological stimulus. In this paper the above mentioned general model was used to account for the effects associated with the second dimension not considered in the previous papers [32,36]; these effects might be important in future validation of proposed model with respect to experimental tests. The size effect of the present 2D investigation consists in the influence of the boundary conditions; due to the lower stimulus at the borders, a more intense remodelling activity occurs far from the edges of the domain, which might be important in the case of metallic implants application. Some numerical simulations for bone samples under plane stress state subjected to uniform in-plane load were presented and commented. These numerical simulations allowed for describing the most desirable situations in which a gradual resorption of the artificial material takes place together with the contemporary formation of new bone, finally giving rise to an almost complete replacement of the artificial material with natural living tissue. In particular, the signal intensity was assumed to decrease exponentially with the distance between sensor cells and actor cells; the effects of adopting two different laws, namely an absolute and a quadratic functions, were compared, showing that the latter causes an increment of the stimulus intensity and hence of the apposition rate of bone. Moreover, a range of load magnitude was identified within

which a physiological state is established: if the load is smaller than the lower bound, resorption of material prevents load transmission, whereas, if load is larger than the upper bound, no change occurs in the distributions of mass densities of bone and material. It was also observed that the growth of the bone begins after the stabilization of the material, at least in the probe point selected. Finally, a parametric analysis was worked out in order to evaluate the sensitivity of the model to variations of some critical quantities, namely resorption rate of material, load magnitude, and homeostatic deformation, within physiological ranges; in more detail, the increments in resorption rate of material and in the load magnitude cause bone formation prevail on material resorption, whereas the decrease of homeostatic deformation causes the opposite effect. The qualitative and quantitative results presented in this paper show that the enhanced model should be able to predict the occurrence of artificial material inclusions or voids in the completely healed reconstructed bones and possibly to optimize the material characteristics with respect to the best regeneration of bone. Finally the importance of the phenomena of load transfer between bone tissue and artificial reinforcement materials used in bone reconstruction should be emphasized: the numerical simulations performed on a two-dimensional sample show how the gradual artificial material replacement is influenced by the modalities with which mechanical strain energy is differently distributed between the pure bone tissue and the bone tissue/artificial material mixture. In this connection it is worth to be emphasized the fact that the two-dimensional model enables us to deal with situations in which it is admitted the onset of local damage, without therefore inevitably producing the failure of the entire sample. From the practical view point during surgery planning and later rehabilitation we have some choice of the following parameters: porosity of the graft, material characteristics of the graft, possibly the choice of the sizes of granules (if granular material is used instead of large piece) and adjustment of initial mixture tissue/granular material and later, during healing and remodelling, loading history. Their influence will be investigated in future works.

References

- [1] U. Andreaus and M. Colloca, Prediction of micromotion initiation of an implanted femur under physiological loads and constraints using the finite element method, *Procs. of the Inst. of Mechanical Engineers. Part H, J. of Engineering in Medicine* **223**(5), 589–605 (2009).
- [2] U. Andreaus, M. Colloca, and D. Iacoviello, Modelling of trabecular architecture as result of an optimal control procedure, Chapter II. In: *Biomedical Imaging and Computational Modeling in Biomechanics* (eds. U. Andreaus and D. Iacoviello), (Springer, 2012), 2012, pp. 19–37.
- [3] U. Andreaus, M. Colloca, and D. Iacoviello, An optimal control procedure for bone adaptation under mechanical stimulus, *Control Engineering Practice* **20**, 575–583 (2012).
- [4] U. Andreaus, M. Colloca, D. Iacoviello, and M. Pignataro, Optimal-tuning pid control of adaptive materials for structural efficiency, *Structural and Multidisciplinary Optimization* **43**(1), 43–59 (2011).
- [5] U. Andreaus, M. Colloca, and A. Toscano, Mechanical behaviour of a prosthesized human femur: a comparative analysis between walking and stair climbing by using the finite element method, *Biophysics and Bioengineering Letters* **1**(3), 1–15 (2008).
- [6] U. Andreaus, F. dell’Isola, and M. Porfiri, Piezoelectric passive distributed controllers for beam flexural vibrations, *Journal of Vibration and Control* **10**(5), 625–659 (2004).
- [7] D. T. J. Barone, J. M. Raquez, and P. Dubois, Bone-guided regeneration: from inert biomaterials to bioactive polymer (nano)composites, *Polym. Adv. Technol.* **22**, 463–475 (2011).
- [8] M. Berry, Development of bioresorbable composite materials for orthopaedic devices, *EMDT - European Medical Device Technology* (2008).
- [9] A. S. Brydone, D. Meek, and S. Maclaine, Bone grafting, orthopaedic biomaterials, and the clinical need for bone engineering, *Proc. IMechE, Part H: J. Engineering in Medicine* **224**, 1329–1343 (2010).
- [10] W. Ching, P. Rulis, and A. Misra, Ab initio elastic properties and tensile strength of crystalline hydroxyapatite, *Acta Biomater.* **5**(8), 3067–3075 (2009).
- [11] S. Cowin, *Bone mechanics handbook* (CRC Press, 2001).
- [12] F. dell’Isola and R. Batra, Saint-Venant’s problem for porous linear elastic materials, *Journal of Elasticity* **47**(1), 73–81 (1997).
- [13] F. dell’Isola, M. Guarascio, and K. Hutter, A variational approach for the deformation of a saturated porous solid. A second gradient theory extending Terzaghi’s effective stress principle, *Archive of Applied Mechanics* **70**(5), 323–337 (2000).
- [14] F. dell’Isola and S. Vidoli, Continuum modelling of piezoelectromechanical truss beams: An application to vibration damping, *Archive of Applied Mechanics* **68**(1), 1–19 (1998).
- [15] F. dell’Isola and S. Vidoli, Damping of bending waves in truss beams by electrical transmission lines with PZT actuators, *Archive of Applied Mechanics* **68**(9), 626–636 (1998).
- [16] V. A. Eremeyev and L. P. Lebedev, Existence of weak solutions in elasticity, *Math. Mech. Solid.* **18**(2), 204–217 (2012).
- [17] D. Farrar, *Bioresorbable polymers in orthopaedics, business briefing: Medical device manufacturing & technology*, Smith & Nephew, www.touchbriefings.com (2005).
- [18] I. Giorgio, A. Culla, and D. D. Vescovo, Multimode vibration control using several piezoelectric transducers shunted with a multiterminal network, *Archive of Applied Mechanics* **79**, 859–879 (2009).
- [19] P. A. Gunatillake and R. Adhikari, Biodegradable synthetic polymers for tissue engineering, *European Cells and Materials* **5**, 1–16 (2003).

- [20] X. Han and J. Pan, A model for simultaneous degradation and crystallisation in biodegradable polymers, *Biomaterials* **30**, 423–430 (2009).
- [21] R. Huang, J. Pan, A. R. Boccaccini, and Q. Chen, A two scale model for simultaneous sintering and crystallization of glass-ceramic scaffolds for tissue engineering, *Acta Biomater.* **4**, 1095–1103 (2008).
- [22] R. Huiskes, H. Weinans, H. J. Grootenboer, M. Dalstra, B. Fudala, and T. J. Slooff, Adaptive bone-remodeling theory applied to prosthetic-design analysis, *J Biomech.* **20**(11-12), 1135–50 (1987).
- [23] C. C. Humber, G. K. B. Sándor, J. M. Davis, S. A. F. Peel, B. M. B. Brkovic, Y. D. Kim, H. I. Holmes, and C. M. L. Clokie, Bone healing with an in situ-formed bioresorbable polyethylene glycol hydrogel membrane in rabbit calvarial defects, *Oral and Maxillofacial Implants* **109**(3) (2010).
- [24] S. J. Jones, A. Boyde, and N. N. Ali, The resorption of biological and non-biological substrates by cultured avian and mammalian osteoclasts, *Anat. Embryol. (Berl.)* **170**, 247–256 (1984).
- [25] A. R. Jr. Santos, *Bioresorbable polymers for tissue engineering*, Tissue Engineering, Daniel Eberli (ed.), ISBN: 978-953-307-079-7, InTech, Available from: <http://www.intechopen.com/books/tissue-engineering/bioresorbable-polymers-for-tissue-engineering> pp. 225–246 (2010).
- [26] R. E. Jung, V. Kokovic, M. Jurisic, D. Yaman, K. Subramani, and F. E. Weber, Guided bone regeneration with a synthetic biodegradable membrane: a comparative study in dogs, *Clin. Oral Impl. Res.* **22**, 802–807 (2011).
- [27] K. Kanayama, W. Sriarj, H. Shimokawa, K. Ohya, Y. Doi, and T. Shibusani, Osteoclast and osteoblast activities on carbonate apatite plates in cell cultures, *Biomater. Appl.* **26**, 435–449 (2011).
- [28] J. Klein-Nulend, P. J. Nijweide, and E. H. Burger, Osteocyte and bone structure, *Current Osteoporosis Reports* **1**, 5–10 (2003).
- [29] J. Klein-Nulend, A. Van der Plas, C. M. Semeins, N. E. Ajubi, J. A. Frangos, P. J. Nijweide, and E. H. Burger, Sensitivity of osteocytes to biomechanical stress in vitro, *The FASEB Journal* **26**, 441–445 (1995).
- [30] G. M. Kontakis, J. E. Pagkalos, T. I. Tosounidis, J. Melissas, and P. Katonis, Bioabsorbable materials in orthopaedics, *Acta Orthop. Belg.* **73**, 159–169 (2007).
- [31] T. Lekszycki, Modelling of bone adaptation based on an optimal response hypothesis, *Meccanica* **37**, 343–354 (2002).
- [32] T. Lekszycki and F. dell’Isola, A mixture model with evolving mass densities for describing synthesis and resorption phenomena in bones reconstructed with bio-resorbable materials, *ZAMM, Z. Angew. Math. Mech.* **92**(6), 426–444 (2012).
- [33] L. H. Li, K. P. Kommareddy, C. Pilz, C. R. Zhou, P. Fratzl, and I. Manjubala, In vitro bioactivity of bioresorbable porous polymeric scaffolds incorporating hydroxyapatite microspheres, *Acta Biomater.* **6**, 2525–2531 (2010).
- [34] A. Madeo, I. Djeran-Maigre, G. Rosi, and C. Silvani, The effect of fluid streams in porous media on acoustic compression wave propagation, transmission, and reflection, *Continuum Mechanics and Thermodynamics* (2012).
- [35] A. Madeo, D. George, T. Lekszycki, M. Nierenberger, and Y. Rémond, A second gradient continuum model accounting for some effects of micro-structure on reconstructed bone remodeling, *Comptes Rendus Mécanique* **340**(8), 575–589 (2012).
- [36] A. Madeo, T. Lekszycki, and F. dell’Isola, A continuum model for the bio-mechanical interactions between living tissue and bio-resorbable graft after bone reconstructive surgery, *Comptes Rendus Mécanique* **339**(10), 625–640 (2011).
- [37] O. Marangos, A. Misra, P. Spencer, B. Bohaty, and J. Katz, Physico-mechanical properties determination using microscale homotopic measurements: application to sound and caries-affected primary tooth dentin, *Acta Biomater.* **5**(4), 1338–1348 (2009).
- [38] C. Maurini, F. dell’Isola, and D. Del Vescovo, Comparison of piezoelectronic networks acting as distributed vibration absorbers, *Mechanical Systems and Signal Processing* **18**(5), 1243–1271 (2004).
- [39] C. Maurini, J. Pouget, and F. dell’Isola, On a model of layered piezoelectric beams including transverse stress effect, *International Journal of Solids and Structures* **41**(16-17), 4473–4502 (2004).
- [40] C. Maurini, J. Pouget, and F. dell’Isola, Extension of the Euler-Bernoulli model of piezoelectric laminates to include 3D effects via a mixed approach, *Computers and Structures* **84**(22-23), 1438–1458 (2006).
- [41] A. Misra, O. Marangos, R. Parthasarathy, and P. Spencer, Micro-scale analysis of compositional and mechanical properties of dentin using homotopic measurements, in: *Biomedical Imaging and Computational Modeling in Biomechanics*, edited by U. Andreaus and D. Iacoviello, *Lecture Notes in Computational Vision and Biomechanics Vol. 4* (Springer Netherlands, 2013), pp. 131–141.
- [42] M. Mullender, A. J. El Haj, Y. Yang, M. A. van Duin, E. H. Burger, and J. Klein-Nulend, Mechanotransduction of bone cells in vitro: mechanobiology of bone tissue, *Med. Biol. Eng. Comput.* **42**, 14–21 (2004).
- [43] S. Narang and V. Chava, Biomaterials used as bone graft substitutes, *Annal Dent. Univ. Malaya* **7**, 36–42 (2000).
- [44] P. Nygaard-Østby, V. Bakke, O. Nerdal, C. Susin, and M. E. U. Wikesjö, Periodontal healing following reconstructive surgery: effect of guided tissue regeneration using a bioresorbable barrier device when combined with autogenous bone grafting. A randomized-controlled trial 10-year follow-up, *J Clin Periodontol* **37**, 366–373 (2010).
- [45] J. Pan, H. X., W. Niu, and R. Cameron, A model for biodegradation of composite materials made of polyesters and tricalcium phosphates, *Biomaterials* **32**, 2248–2255 (2011).
- [46] R. Parthasarathy, A. Misra, J. G. Park, Q. Ye, and P. Spencer, Diffusion coefficients of water and leachables in methacrylate-based crosslinked polymers using absorption experiments, *J. Mater. Sci. Mater. Med.* **23**(5), 1157–1172 (2012).
- [47] S. Quiligotti, G. A. Maugin, and F. dell’Isola, An eshelbian approach to the nonlinear mechanics of constrained solid-fluid mixtures, *Acta Mechanica* **160**(1-2), 45–60 (2003).
- [48] G. Rosi, I. Giorgio, and V. A. Eremeyev, Propagation of linear compression waves through plane interfacial layers and mass adsorption in second gradient fluids, *ZAMM, Z. Angew. Math. Mech.* pp. 1–14 (2013).
- [49] G. Rosi, R. Paccapeli, F. Ollivier, and J. Pouget, Optimization of piezoelectric patches positioning for passive sound radiation control of plates, *J. Vib. Control* (2012).

- [50] G. Rosi, J. Pouget, and F. dell'Isola, Control of sound radiation and transmission by a piezoelectric plate with an optimized resistive electrode, *Eur. J. Mech. A-Solids* **29**(5), 859–870 (2010).
- [51] C. T. Rubin and L. E. Lanyon, Osteoregulatory nature of mechanical stimuli: Function as a determinant for adaptive remodeling in bone, *Journal of Orthopaedic Research* **5**, 300–310 (1987).
- [52] R. Ruimerman, P. Hilbers, B. van Rietbergen, and R. Huiskes, A theoretical framework for strain-related trabecular bone maintenance and adaptation, *J. Biomechanics* **38**, 931–941 (2005).
- [53] G. Sciarra, F. dell'Isola, and K. Hutter, A solid-fluid mixture model allowing for solid dilatation under external pressure, *Continuum Mechanics and Thermodynamics* **13**(5), 287–306 (2001).
- [54] Y. Shikinami, Y. Matsusue, and T. Nakamura, The complete process of bioresorption and bone replacement using devices made of forged composites of raw hydroxyapatite particles/poly l-lactide (F-u-HA/PLLA), *Biomaterials* **26**(27), 5542–51 (2005).
- [55] J. A. Simon, J. L. Ricci, and P. E. Di Cesare, Bioresorbable fracture fixation in orthopedics: a comprehensive review. Part I. Basic science and preclinical studies, *Am J Orthop (Belle Mead NJ)* **26**(10), 665–71 (1997).
- [56] J. A. Simon, J. L. Ricci, and P. E. Di Cesare, Bioresorbable fracture fixation in orthopedics: a comprehensive review. Part II. Clinical studies, *Am J Orthop (Belle Mead NJ)* **26**(11), 754–62 (1997).
- [57] H. Tsuji, Autocatalytic hydrolysis of amorphousmade polylactides: Effects of L-lactide content, tacticity, and enantiomeric polymer blending, *Polymers* **43**, 1789–1796 (2002).
- [58] M. L. Wang, J. Massie, A. Perry, S. R. Garfin, and C. W. Kim, A rat osteoporotic spine model for the evaluation, of bioresorbable bone cements, *The Spine Journal* **7**, 466–474 (2007).
- [59] Y. Wang, X. Han, J. Pan, and C. Sinka, An entropy spring model for Young's modulus change of biodegradable polymers during biodegradation, *Journal of the Mechanical Behaviour of Biomedical Materials* **3**, 14–21 (2010).
- [60] Y. Wang, J. Pan, X. Han, C. Sinka, and L. Ding, A phenomenological model for the degradation of biodegradable polymers, *Biomaterials* **29**, 3393–3401 (2008).